Developing climate services for vulnerable islands in the Southwest Indian Ocean: A combined statistical and dynamical CMIP6 downscaling approach for climate change assessment

Marie-Dominique Leroux, François Bonnardot, Samuel Somot, Antoinette Alias, Stephason Kotomangazafy, Abdoul-Oikil Saïd Ridhoine, Philippe Veerabadren, Vincent Amélie

Graphical Abstract

Advancing Climate Services for Vulnerable Islands in the Southwest Indian Ocean: A Combined Approach of Statistical and Dynamical CMIP6 Downscaling

Marie-Dominique Leroux, François Bonnardot, Samuel Somot, Antoinette Alias, Stephason Kotomangazafy, Abdoul-Oikil Saïd Ridhoine, Philippe Veerabadren, Vincent Amélie

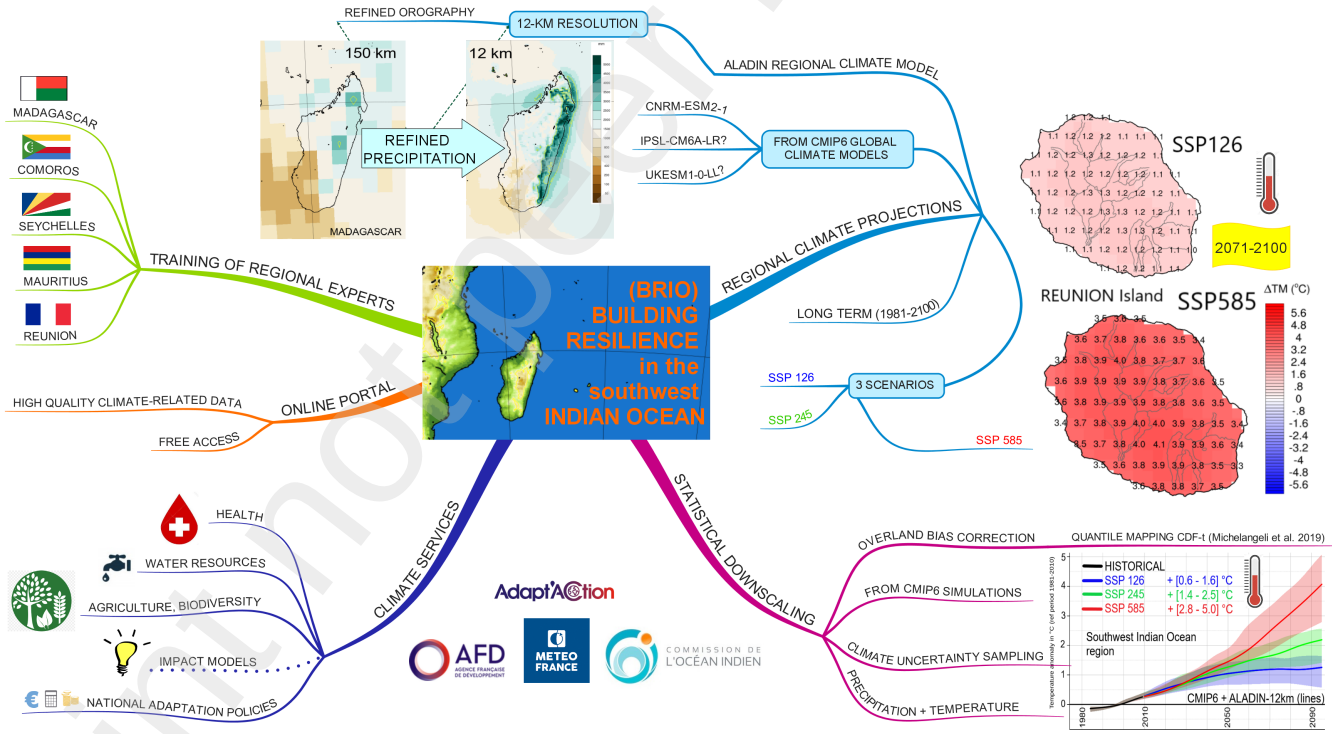

Highlights

Advancing Climate Services for Vulnerable Islands in the Southwest Indian Ocean: A Combined Approach of Statistical and Dynamical CMIP6 Downscaling

Marie-Dominique Leroux, François Bonnardot, Samuel Somot, Antoinette Alias, Stephason Kotomangazafy, Abdoul-Oikil Saïd Ridhoine, Philippe Veerabadren, Vincent Amélie

- Multiple approaches to produce climate services within a resource-constrained context
- A potential framework model for other vulnerable regions with limited CORDEX coverage
- A dry season expected to become drier in most of the Southwest Indian Ocean
- An expected increasing tropical cyclone risk per event in the Southwest Indian Ocean

Advancing Climate Services for Vulnerable Islands in the Southwest Indian Ocean: A Combined Approach of Statistical and Dynamical CMIP6 Downscaling

Marie-Dominique Leroux[a,*], François Bonnardot[a], Samuel Somot[b], Antoinette Alias[b], Stephason Kotomangazafy[c], Abdoul-Oikil Saïd Ridhoine[d], Philippe Veerabadren[e], Vincent Amélie[f]

[a]*Météo-France, Direction Interrégionale pour l'Océan Indien, 97490 Saint-Denis de La Réunion, France*
[b]*CNRM, Université de Toulouse, Météo-France, CNRS, Toulouse, France*
[c]*Direction Générale de la Météorologie, Madagascar*
[d]*Agence Nationale de l'Aviation Civile et de la M´et´eorologie (ANACM), Moroni, Comores*
[e]*Mauritius Meteorological Services, Maurice*
[f]*Seychelles Meteorological Authority, Seychelles*

Abstract

Climate change is a global challenge that requires local solutions. Small island developing states (SIDS) in the southwest Indian Ocean (SWIO) basin are particularly vulnerable and already facing significant challenges due to climate variability and extreme weather events like tropical cyclones (TCs). Tailored climate services, catering to their specific needs and contexts, are crucial for formulating appropriate adaptation strategies. This study aims to fill the gap of localized and reliable information for climate services in the SWIO region. Climate data is dynamically downscaled at kilometer-scale resolution over numerous islands from a 12-km resolution regional climate

*Corresponding author
Email address: mariedominique.leroux@gmail.com (Marie-Dominique Leroux)

model that represents the climatology of tropical cyclones. A subset of the latest CMIP6 simulations is also statistically downscaled over La Réunion to quantify model uncertainties. Daily mean temperatures over small islands are projected to increase by an average of 1.2°C (SSP1-2.6) to 3.5°C (SSP5-8.5) by the end of the century relative to the reference 1981-2010 period, and up to 4.4°C on Madagascar (SSP5-8.5). The dry season in the SWIO region is anticipated to become significantly drier, with precipitation deficits ranging from 10% to 40%, primarily due to a delayed onset of the rainy season. The cyclonic risk is expected to increase with higher TC intensities, a higher portion of strong TCs, and a poleward migration of TC lifetime maximum intensity, further increasing the risk on the Mascarene islands.
Keywords: Indian Ocean, dynamical downscaling, statistical downscaling, regional climate projections, climate services, heat waves, droughts, climate change, tropical cyclones, Small Island Developing States, La Réunion, Mascarene Islands.

Practical Implications

Climate datasets are expected in inhabited countries of the Southwest Indian Ocean, from both citizens and decision-makers, to address the pressing regional needs for climate services and impact studies. The current needs extend across various climate-sensitive sectors, encompassing agriculture, water resources, health, biodiversity, and the energy sector, with a focus on solar and wind potential to advance energy autonomy across our islands. La Réunion, in particular, has demonstrated a significant need for support in formulating public policies. This includes crucial documents like the Depart-

mental Plan for Water and Hydraulic Development, the Regional Framework for Sustainable Development and Planning, Local Urban Plans, Climate Air Energy Territorial Plans of local communities, reports from the French High Council for Climate, and more.

The Building Resilience in the Indian Ocean (BRIO) project, for the first time to the best of our knowledge, has produced well-documented, fine-scale, timely, reliable, and accessible regional to local climate information for the 21^{st} century tailored for the Indian Ocean Commission (IOC) member countries: Madagascar, La Réunion, Mauritius, Comoros and Seychelles archipelagos. A hierarchy of methods were employed, encompassing regional analysis of CMIP6 models, dynamical downscaling, statistical bias correction, statistical downscaling, computation of user-relevant indices, and delivery in an accessible and understandable format. The BRIO project has also provided training for national experts in climate data mining across these IOC member countries.

0.1. Data availability for climate services initiatives

The BRIO climate data is visible through the regional portal (`http://climat.coi-ioc.org`). Additionally, the regional model outputs are available on the DRIAS portal provided by Météo-France at `http://www.drias-climat.fr/` in the "Accès Simplifié" tab of the "Données et Produits" section. Users can download the raw model outputs at 12-km resolution covering the entire South-West Indian Ocean (SWIO) domain, along with bias-corrected data for daily precipitation, minimum and maximum temperatures in La Réunion and Mayotte. Bias-corrected data for other islands can be obtained by reaching out to IOC-trained experts via the email address provided for the first

author of this paper. The BRIO dataset is recognized for its utility and has already been utilized in numerous impact studies in La Réunion, contributing to the understanding and mitigation of vulnerability to climate risks.

0.2. An example of impact study conducted on La Réunion

We elaborate here on one specific application, assessing anticipated vegetation changes through ombrothermal indices. Additional ongoing applications are listed in Section 0.3. According to the Worldwide Bioclimatic Classification System of Rivas-Martinez and Rivas-Sáenz (1996-2009, www.globalbioclimatics.org), the ombrothermal index should reflect the overall usable water quantity for vegetation in relation to temperature. The standard Martonne index, based on annual inputs, proves inadequeate in La Réunion due to seasonal variations (Appendix A) and cyclonic rains (partially unusable by vegetation due to runoff). In collaboration with the National Botanical Conservatory Mascarin (CBN-CPIE Mascarin), we propose to define the ombroclimate attribute from a vegetation standpoint through daily water balance diagnostics that equalize rainfall and potential evapotranspiration.

The regional climate model (CNRM-ALADIN, presented in section 3) is employed to compute evapotranspiration (ETP) using wind, precipitation, temperature, and solar radiation, corrected with observation datasets. Crop evapotranspiration (ET0) is determined with the FAO 56 Penman-Monteith equation for a grass reference surface [1]. Daily water balance data, accounting for meteorological factors influencing plant water consumption and soil recharge, is calculated in both observations and model outputs. To address cyclonic rains, the soil's easily usable reserve (EUR) is set at 60 mm, and the total usable reserve (UR) at 80 mm. The annual count of days with soil water

(a) HIST 1981-2010

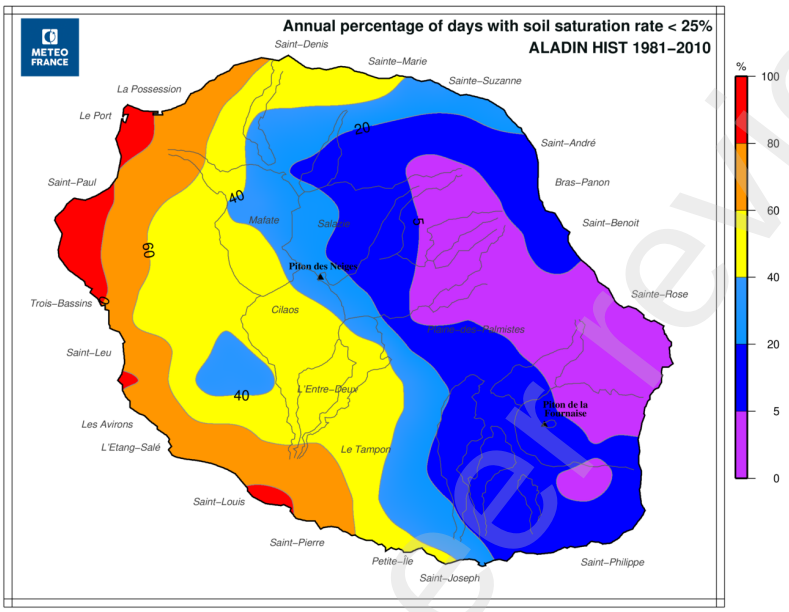

(b) SSP5-8.5 2041-2070

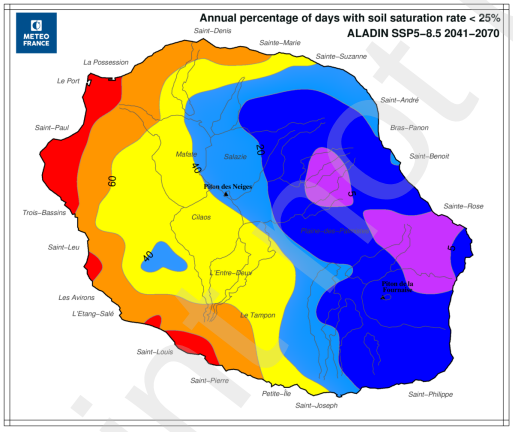

(c) SSP5-8.5 2071-2100

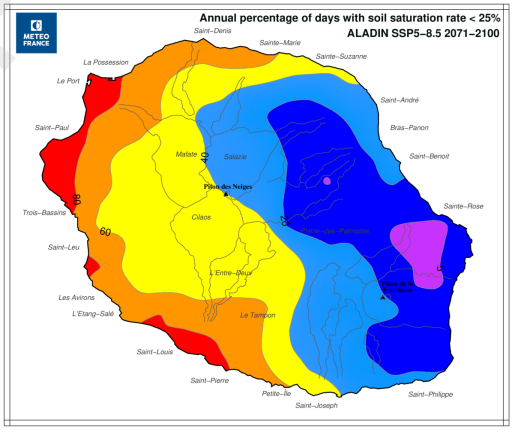

Figure 1: Ombrothermal Index computed using daily water balance from CNRM-ALADIN bias-corrected outputs for (**a**) the historical period 1981-2010 and for the SSP5-8.5 scenario during the time periods (**b**) 2041-2070 and (**c**) 2071-2100. The index categories are based on the annual percentage of days with soil water saturation below 25%, as defined in Table 1.

content below 20 mm indicates vegetation experiencing hydric stress. The cartographic representation of water balance, derived from observations and historical model data, aligns well with vegetation expression, highlighting east-west climate disparities, cirque-specific variations, and gradients along the northern and southern coasts (Fig. 1a). The red area reasonably delineates the so-called savannah region.The red area reasonably delineates the so-called savannah region. The Southwest Highlands' humid areas (Plaine des Makes, Tévelave) are discernible. Classes for this attribute are detailed in Table 1.

Table 1: Classes for ombroclimate index defined through the water balance.

Percentage of annual days with soil water saturation $< 25\%$	**Biotope class**
0 to 5	hyper-humid
5 to 20	humid
20 to 40	semi-humid
40 to 60	semi-arid
60 to 80	arid
80 to 100	hyper-arid

Figures 1b and 1c show vegetation changes under the driest SSP5-8.5 scenario. Anticipated impacts include a reduction in very humid zones in the east, expansion of arid areas to higher altitudes (westward savannah growth), and challenges for the semi-humid Plaine des Makes zone by the end of the century (disappearance of the blue triangle).

0.3. Other impact studies using the BRIO dataset

Studied impact	**Daily BRIO variables**	**Collaborator**	**Reference**
Vegetation change and ombrothermal indices	water balance assessments using evapotranspiration (ETP) computed from wind, RR, TN, TX, and solar radiation	CBN-CPIE Mascarin	Section 0.2
Aedes Albopictus mosquito populations (dynamics of dengue fever epidemics)	TN, TX, RR	LACy, CIRAD	[44], currently expanding to other IOC islands
Gene expression and vector competence of tiger mosquitoes (dengue serotypes)	TN, TX, RH, RR, solar radiation	PIMIT	Ongoing
Zoonosis (Leptospirosis)	TN, TX, RR	PIMIT, CIRAD	Ongoing project over various IOC islands
Invasive exotic species	TN, TX, RR	PVBMT	Ongoing
Solar, wind and hydrogen energy production	solar radiation, TN, TX, 50- to 150-m winds, RH, disaggregated at an hourly time step	EnergyLab	[65] and ongoing project

Building thermal comfort	TN, TX, RH, 10-m wind, disaggregated at an hourly time step	PIMENT	Ongoing
Sugarcane cultivation and shifs in crop calendars	water balance assessments using evapotranspiration (ETP) computed from wind, RR, TN, TX, and solar radiation	CIRAD, TEREOS	[9]
Wildfire prevention	computation of meteorological fire indices	wildfire protection services	Ongoing
Tree species	TN, TX, RR, RH, 10-m wind	National Forestry Office (ONF)	Ongoing

Table 2: Utilization of the BRIO dataset in select impact studies conducted in La Réunion, focusing on minimum (TN) and maximum (TX) temperatures, relative humidity (RH), precipitation (RR), winds and solar radiation. LACy, PIMIT, PVBMT, PIMENT, and EnergyLab are all laboratories affiliated with La Réunion University.

1. Introduction

Climate change is a global challenge with far-reaching consequences, impacting both the environment and society [36]. Regions like the SWIO are particularly vulnerable, hosting numerous small island developing states facing climate-related challenges [47, 21]. This vulnerability is exacerbated by the frequent occurrence of extreme weather events, including tropical cyclones [46]. The SWIO basin, spanning from 30 to 90 degrees East, experiences an average of 9.7 tropical systems annually, with 4.8 developing into tropical cyclones (TCs) that are equivalent to a hurricane or a typhoon [46].

The Southwest Indian Ocean region is not immune to the impacts of climate change. Observational records from Meteo-France reveal a clear significant warming trend of +0.17°C per decade over the past six decades on La Réunion (Fig. 2). On the Comoros Archipelago (including Mayotte), near-surface (2 m) air temperatures have risen at a significant rate of +0.19°C per decade. These warming trends are not strictly linear and the warming has intensified in the recent two decades (Fig.2). Moreover, changes in precipitation patterns are evident, with a 36% decrease in annual precipitation in the southwest region of La Réunion over the past 60 years (Appendix B). On Mayotte, dry-season precipitation (May to October) has experienced a 33% decline during the same period (Appendix B).

The Indian Ocean's most rapid sea surface temperature (SST) warming since the 1950s, highlighted by the IPCC [29], raises concerns about the evolution of tropical cyclones in the SWIO basin. Over the past 41 years, there is no significant trend in the number of observed tropical systems (Appendix C). However, while ongoing reanalysis at the Regional Specialized

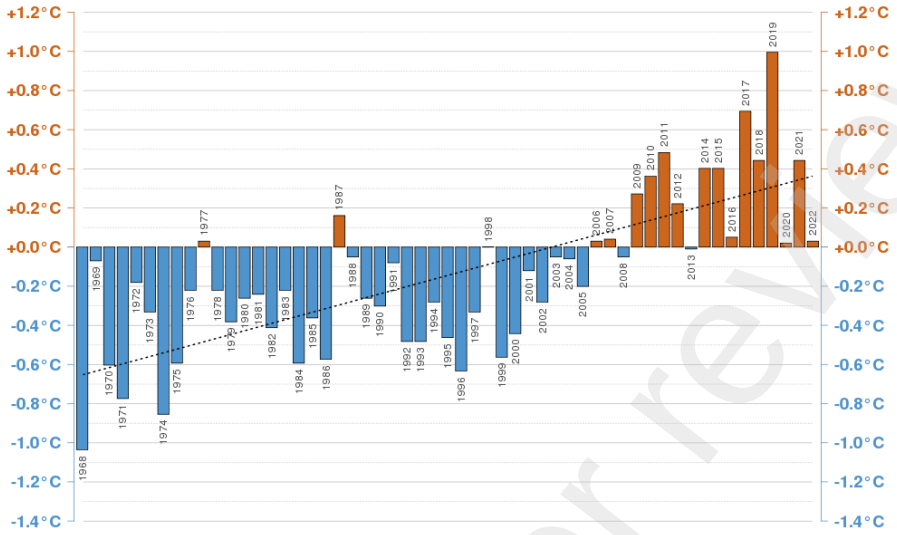

Figure 2: Evolution of the observed average annual near-surface (2 m) air temperature anomaly from 1968 to 2022, relative to the homogenized 1991-2020 baseline, across La Réunion (thermal indicator based on data from 3 weather stations).

Meteorological Center (RSMC) of La Réunion is assessing TC intensity, [27] already reported an increase in Category 5 cyclones. Globally, [41] noted a rise in the proportion of Category 3-5 TC instances to all Category 1-5 instances over the past four decades. Additionally, [42] identified a poleward migration of TC maximum intensity. From reconstructed long-term proxy data and high-resolution climate simulations, [15] revealed a 13% reduction in global cyclone frequency between 1850-1900 and 1900-2000.

Summarizing TC projections for the late 21st century, [40] suggests a 14% decrease in global TC frequency for a 2°C global warming. This reduction is prominent in weaker storms. Global-scale projections anticipate increased TC rain rates due to rising SSTs and environmental water vapor, aligning with Clausius-Clapeyron scaling [16, 40]. The intensification of the strongest

TCs is also projected [25, 41]. Medium- to high-resolution climate projections for the South Indian Ocean align with the global trend, indicating a decrease in overall TC frequency and an increase in intense TC frequency in response to global warming [53, 70, 14, 40, 67]. For a 2°C warmer world, [14] projects a 20% decrease in Southern Indian Ocean TC frequency, with an increased maximum intensity, poleward shift of lifetime maximum intensity, and delayed cyclone season onset. Using a pseudo global warming approach, [67] projects a 6.5% average intensity increase, a 2-degree poleward shift, and a 33.8% rise in median rainfall rates under a scenario of 1.1°C to 4.2°C sea surface temperature warming (RCP 8.5). A recent study by [7] highlight an increasing TC risk at landfall over the South Indian basin and in coastal cities, including Saint-Denis in La Réunion.

Small island states and developing countries in the SWIO face multiple risks beyond tropical cyclones, including droughts and heat waves, impacting water resources and health, notably in Madagascar [43, 32, 71, 55, 2] and the Comoros Archipelago. Recognizing the unique challenges of these islands, the Intergovernmental Panel on Climate Change (IPCC) prioritizes downscaling for developing specific models for these island territories in its latest report [37]. Addressing the vulnerability, there's a growing recognition of the need for climate services to aid adaptation in these regions. Climate services involve providing climate information and analysis for decision-making in climate-sensitive sectors. Such research focus is crucial given the limited availability of climate services in the SWIO region.

The Coupled Model Inter-comparison Project phase 6 (CMIP6) multi-model ensemble [57, 26] offers valuable data for SWIO climate projections,

but its coarse global models may struggle to capture intricate interactions between the ocean, atmosphere, and land that are essential for accurate small island climate simulation. Global models may also inadequately represent tropical cyclones, introducing biases and uncertainties into projections. Studies emphasize the need for high resolution to simulate realistic TCs and project changes in intense TC frequency [52, 60, 20, 12]. [61] highlights the added value of regional climate modeling in regions with complex terrain, land-sea contrasts, and extreme events. The former Coordinated Regional Climate Downscaling Experiment (CORDEX) program, based on CMIP5 models, used a coarse 50 km resolution for Africa and Asia but only a finer 12 km resolution for Europe. A 50-km resolution is inadequate for small and steep islands like those in the SWIO: the biggest island, La Réunion, measures approximately 75 x 55 km along its diagonals, and peaks at almost 3100 m high. Additionally, CORDEX-Africa and CORDEX-SouthAsia, covering only parts of the SWIO basin, fail to represent the climatology of tropical systems across the entire region, limiting their utility for impactful climate studies. In summary, existing CORDEX domains fall short in size and resolution to effectively cover the SWIO region. Gaps in the climatic representation of small island states highlight the pressing need for high-resolution, localized climate data and models. This study, preceding the CMIP6-based CORDEX initiative, seeks to bridge this gap by providing precise and reliable climate information tailored to the unique challenges of the SWIO region.

Our study explores tailoring CMIP6 data for stakeholders in the SWIO region. The focus on La Réunion aims to demonstrate the potential benefits of producing climate services for small island territories. The CNRM-

ALADIN model with 12 km resolution is used to downscale CNRM-ESM2-1 from CMIP6 for three emission scenarios. The analysis also employs 22 CMIP6 models to gauge confidence in temperature and precipitation projections. Our study is unique in several respects. First, we focus on a region that has received relatively little attention in previous studies of regional climate change, probably because the CORDEX initiative has focused mainly on continental areas. Second, we use state-of-the-art climate models to simulate the regional climate of the southwest Indian Ocean basin, providing a more detailed and accurate picture of how the climate is likely to change in the future. Third, we employ a hybrid of dynamical and statistical downscaling, integrating bias correction and spatial disaggregation methods to create high-resolution CMIP6-based climate projections. This approach caters to local stakeholders and decision-makers as it considers model uncertainty. Fourth, our study covers a vast area from the east coast of Africa to 74°E, capturing the primary tropical cyclone genesis region for a comprehensive understanding of precipitation patterns. Fifth, we assess projected changes in SWIO cyclone activity through detailed high-resolution simulations.

This article follows this structure: Section 2 presents observational datasets and the CMIP6 global model dataset. Section 3 details dynamical downscaling, statistical downscaling over La Réunion, the bias correction method and tracking algorithm. Section 4 assesses model and method performance, and presents key climate outcomes (temperature, heatwaves, precipitation, cyclonic activity). Section 5 discusses the results and offers recommendations for future studies. Section 6 summarizes the key findings.

2. Data

2.1. Reference datasets

We used in-situ meteorological daily measurements that have homogeneous long series on Madagascar, Réunion, Seychelles, Comoros, Mayotte, Mauritius, Rodrigues, Agalega, and St Brandon. Kriging, a geostatistical interpolation technique, smoothed data over islands like Réunion, Seychelles, and Mauritius, providing gridded datasets.

For La Réunion, precipitation were interpolated onto a 0.03° grid (about 3 km), covering 1981 to present with 78 rain gauges. Simple kriging, considering inverse distance, was employed. The altitude predictor wasn't pertinent at the daily time step due to the high spatial and temporal variabilities of precipitation on the island (Appendix A). Spatialized normals for daily minimum and maximum near-surface air temperatures were obtained from the climate atlas [38], integrating predictors like distance to the coast, slope, and exposure [Aurelhy method, 23]. Observations, including daily minimum and maximum near-surface (2 m) temperatures, were spatialized across the island using a 250 m resolution digital elevation model. Bessafi et al. [6] provides a detailed description of the method used for the radiation variable. Daily meteorological parameters like near-surface (10 m) wind speed, global radiation, and near-surface minimum and maximum humidity were also spatialized, aiding potential evapotranspiration (ETP) calculations, especially for agriculture.

In Madagascar, the dataset has a unique feature, combining satellite and in-situ observations due to the island's size and rugged terrain. Developed through the Maproom Climate Information Service of Madagascar [59], it is

interpolated on a 4 km (0.0375°) grid. Leveraging CHIRPS [Climate Hazards Group InfraRed Precipitation with Stations, 30], it uses a modified inverse distance weighting approach for interpolation. The combined dataset from Maproom used here is distinct from CHIRPS as it employs 25 rain gauges with less than 30% missing data out of the 189 available observation stations. Maproom, an online mapping service that provides climate information tools, can be accessed at http://www.meteomadagascar.mg/maproom. Rigorous quality control, using IRI-Climate Data Tools (IRI-CDT, `https://github.com/rijaf-iri/CDT`) ensures data reliability and homogeneity [59].

The best track (BT) dataset from RSMC La Réunion stores observed track and 10-minute wind speed intensity of cyclonic events and is an up-to-date version of IBTrACS [`https://www.ncdc.noaa.gov/ibtracs/`, 39]. Due to the absence of aircraft reconnaissance in the SWIO basin, forecasters at RSMC La Réunion employ the Dvorak technique [24] on satellite imagery for storm center and intensity estimation. A tropical depression is assigned a name and becomes a tropical storm (TS) when its 10-minute maximum sustained wind speed (VMAX) reaches 34 knots. Subsequent intensification stages are tropical cyclone (TC, VMAX >= 64 kt), intense tropical cyclone (ITC, VMAX >= 90 kt), and very intense tropical cyclone (VITC, VMAX > 115 kt), equivalent to Category 4 and 5 storms in the Saffir-Simpson scale. Notably, the Dvorak scale traditionally uses 1-minute sustained winds [68], but in the SWIO basin, a common practice is to apply an empirical factor of 0.88 [72] for conversion to 10-minute sustained wind speeds. Thus, intensity thresholds in the SWIO may correspond to slightly higher TC intensities than the standard Saffir-Simpson scale.

To assess global and regional climate models' performance in capturing the Intertropical Convergence Zone (ITCZ) and related precipitation, we employ the IMERG product [35] at 0.1-degree resolution and ERA5 reanalyses [34] at 0.25-degree resolution. IMERG, a NASA product, provides global precipitation estimates with approximately 10 km spatial resolution over about 20 years, merging data from microwave and infrared sensors. Monthly rain gauge measurements correct biases in satellite estimates in the used Final run product. Although IMERG products show satisfactory performance in detecting spatial variability and a 62% accuracy rate for reconstructed precipitation in hurricane studies [56], they tend to underestimate high-intensity precipitation during tropical cyclones [73]. An evaluation of precipitation climatology in IMERG and ERA5 datasets over La Réunion is detailed in Appendix D.

2.2. CMIP6 ensemble for representing modeling uncertainty

A CMIP6 ensemble [historical and ScenarioMIP, 57, 26] was chosen to represent modeling uncertainty in temperature and precipitation projections over the century in the SWIO basin. The selected ensemble comprises 22 global climate models from the CMIP6 archive (`https://esgf-node.llnl.gov/search/cmip6/`), providing daily data for precipitation, temperature, and wind variables for at least the two extreme scenarios (SSP1-2.6 and SSP5-8.5) at the time of the study.

Unlike a performance-based model selection for specific regions [e.g, 58, 31], our approach aimed to maintain model diversity and the filtered projection range. We evaluated the potential range of changes in surface temperature and precipitation across the SWIO region. Screening for the CMIP6

ensemble involved considering the IPCC AR6 likely range for Equilibrium climate sensitivity (ECS) and/or Transient climate response (TCR) [33]. ECS and TCR values, critical metrics for comparing model responses to greenhouse gas changes, can be found in [28, 36] or in [49] or in Appendix A of [63]. Concerns about a subset of CMIP6 models with higher climate sensitivities, potentially leading to misleading temperature projections, have been raised in previous studies [e.g., 62, 33, 63]. Among the 22 models used, 7 (BCC-CSM2-MR, CAMS-CSM1-0, CNRM-ESM2-1, FGOALS-g3, MIROC6, MRI-ESM2-0, NorESM2-LM) belong to the low ECS (1.83–3.02°C) or low TCR (1.22–1.83°C) GCM sub-ensemble recommended for effective use in climate change policy [63].

When selecting a global model for driving the regional model (CNRM-ALADIN), we excluded unrealistic and highly sensitive models for a more accurate representation of the regional climate. Subsection 4.3 offers a detailed overview of our selection process. CNRM-ESM2-1, part of the sub-ensemble of 7 low-ECS or low-TCR GCMs, aligns with the median range of the 22 CMIP6 models in terms of temperature evolution, thereby offering a balanced and reliable choice. It also belongs to the group of models displaying the most significant reduction in future precipitation in the region. This characteristic makes it a valuable choice for addressing severe risks related to water resources. The use of a suite of CNRM models ensures consistency between the GCM and the regional climate model (RCM), sharing the same dynamical core, physical parameterizations, and forcings [66, 8]. CNRM-ESM2-1, also assessed for its capability to represent present-day tropical climate processes in the SWIO region, was therefore retained to

drive the regional model.

3. Methods

3.1. Dynamical downscaling

Dynamical downscaling from CMIP6 simulations [historical and ScenarioMIP, 57, 26] was employed to derive regional climate information for a vast area in the southwest Indian Ocean, covering most inhabited countries from Mozambique's coasts (33°E) to 74°E, including the main tropical cyclone genesis area [2-28°S]. Implemented in its latest 6.3 climate version [54], the CNRM-ALADIN limited area model features a 12 km horizontal resolution and 91 vertical levels. It is based on a bi-spectral, semi-implicit, semi-Lagrangian advection scheme and shares its dynamical core with the global model CNRM-ESM2-1 [64]. The CNRM-ALADIN simulations were driven by CNRM-ESM2-1, which has a resolution of approximately 150 km (T127) and 91 vertical levels. The atmospheric lateral boundary forcing was provided at 6-h frequency. Historical simulations covered 1979-2014, while projections spanned SSP1-2.6, SSP2-4.5, and SSP5-8.5 scenarios [57, 50] from 2015 to 2100. The acronym "SSPX-Y.Y" denotes Shared Socioeconomic Pathways (SSP) with a development pathway X (1, 2, 3, 4, or 5) leading to a net radiative Y.Y by 2100 [50]. The fine spatial resolution of CNRM-ALADIN captures terrain details and coastlines (shown later in section 4.6), crucial for representing small islands like Seychelles, Comoros, and the Mascarene islands (La Réunion, Mauritius, Rodrigues), ensuring a more accurate depiction of their topography and precipitation patterns.

Our analysis uses Global Warming Levels (GWLs) derived from the CNRM-ESM2-1 model projections to anticipate future trends in tropical cyclones and precipitation. Calculated over 30-year intervals in the 21st century, GWLs quantify average climate changes relative to the pre-industrial era (1850-1900). To assess regional changes, we compare CNRM-ALADIN output values within these 30-year periods to those of the baseline 1981-2010 period for CNRM-ALADIN.

3.2. Tropical system tracking and intensity correction

Tropical systems in CNRM-ALADIN are tracked every 6 hours using the algorithm introduced and detailed in [18], and later used in [19, 17, 14]. Each cyclone is represented by a series of latitude-longitude points and its intensity is defined by the maximum 10m wind speed.

The maximum cyclone intensities from CNRM-ALADIN's historical data (1981-2010) were compared with BT data (1985-2014). A correction method was used to address intensity discrepancies. Quantile-quantile correction first aligned the distribution of lifetime maximum intensities in the modeled systems with the BT data. After correcting maximum wind values, a linear regression recalibrated each wind value based on the new maximum and minimum intensity values of each system. This ensured consistency in cyclone intensities between the regional model and the reference dataset. Similar corrections were applied to projections.

The Accumulated Cyclone Energy index (ACE), widely used to gauge system or seasonal cyclonic activity and assess long-term trends [e.g., 5, 11, 4], is a more comprehensive risk indicator than storm frequency or intensity alone. It better correlates with economic damages. ACE is calculated by

summing the square of the maximum sustained wind speed (in knots) at six-hour intervals for all periods with at least TS-force winds (VMAX >= 34 kt). Seasonal or annual ACE values reflect the combined duration, strength, and frequency of tropical systems.

3.3. Bias correction method applied on islands

A statistical correction method is crucial in climate simulations for impact studies and climate indicators, especially when climate projections show biases compared to observations. This correction aligns simulated and observed data, improving the reliability of climate assessments. The method used here corrects the simulated distribution for each variable seasonally. Bias correction was applied to both past (1981-2014) and future (2015-2100) periods using 30-year moving time-slices over 3-month windows centered on the month to correct. The Cumulative Distribution Function-transform (CDF-t) bias correction algorithm was chosen because it accounts for changes in CDF relative to the calibration period. CDF-t, initially developed for wind speed bias correction and downscaling [51], has also been applied to temperature or precipitation [69, 45].

After bias correction, the final resolution depends on observational data and ranges from about 4 km (Madagascar, Mauritius) to 3 km (Réunion) for gridded data. Station-scale bias correction was applied on smaller islands like Seychelles, Comoros, Mayotte, Rodrigues, Agalega, and St Brandon. Bias correction for humidity, wind, and solar radiation reference parameters was conducted at a 3-km resolution over Réunion Island to facilitate daily evapotranspiration calculation using the FAO-56 formula [1].

3.4. Statistical downscaling on La Réunion

Statistical downscaling was performed on La Réunion using 22 CMIP6 model simulations to assess model uncertainty of temperature and precipitation variables and derived climate indices. For daily precipitation, the CDF-t bias correction was computed in different atmospheric conditions. This involved categorizing five 850-hPa wind classes that capture diverse weather regimes affecting precipitation distribution over the island. These classes align with the four wind sectors: North, East, South, and West, with a fifth class for winds below 2.7 m/s.

Unlike precipitation, temperature variations are less influenced by weather types and primarily operates on a larger scale, so statistical downscaling of minimum and maximum temperatures was performed using the CDF-t method without considering weather types.

4. Results

4.1. Evaluation of the statistical downscaling method

The statistical downscaling method is evaluated on ERA5 reanalyses for 1981-2017, divided into a training period (1981-2010) and a testing period (2011-2017). The model is calibrated during the training period using historical data, while the testing period assesses the model's performance and its ability to accurately downscale precipitation. The ERA5 data is degraded to a 1° resolution to align with the typical resolution of CMIP6 models. The benefit of using the 5 classes of 850 hPa wind sectors (BC-WT) is compared to applying the CDF-t correction on the entire dataset (BC). Quantile-quantile

(QQ) plots are generated for each wind sector type and each method to assess the improvement. Specific weather situations, including southward flow (winter cold fronts or trough situations), eastward flow (trade winds), and northward flow (tropical systems) are examined. For each scenario, the observed precipitation is compared with the ERA5 bias-corrected precipitation obtained with or without using wind regimes. For instance, for southward flow, a significant enhancement of precipitation on the southern side of the island is observed when applying wind sector correction, consistent with the observed behavior (e.g., Fig.3).

The Taylor diagram is used to evaluate and compare the performance of the models against observed data at each grid point. The two main models evaluated are ERA5 after simple bias correction (ERA5-BC) and ERA5 after bias correction using wind-based time regimes (ERA5-BC-WT). Plotted for comparison is the ERA5 analysis interpolated at 0.03° resolution (ERA5). For each model, the correlation and standard deviation values averaged over all grid points are represented by large squares on the diagram (Fig. 4). The uncorrected ERA5 data exhibit less variability than observed (Fig. 4a), leading to underestimation of extreme events (see also Appendix D). However, after bias correction, the standard deviations of ERA5-BC and ERA5-BC-WT become comparable to those of the observations (Fig. 4a), indicating successful introduction of variability in the models.

ERA5-BC-WT, which corrects biases based on wind sectors, shows slightly higher average performance across all grid points (Fig. 4a) and outperforms ERA5-BC on more than half of the grid points. The models' improvements are consistent and maintain their validity over the independent validation

(a) ERA5 at 1° resolution

(b) OBSERVED

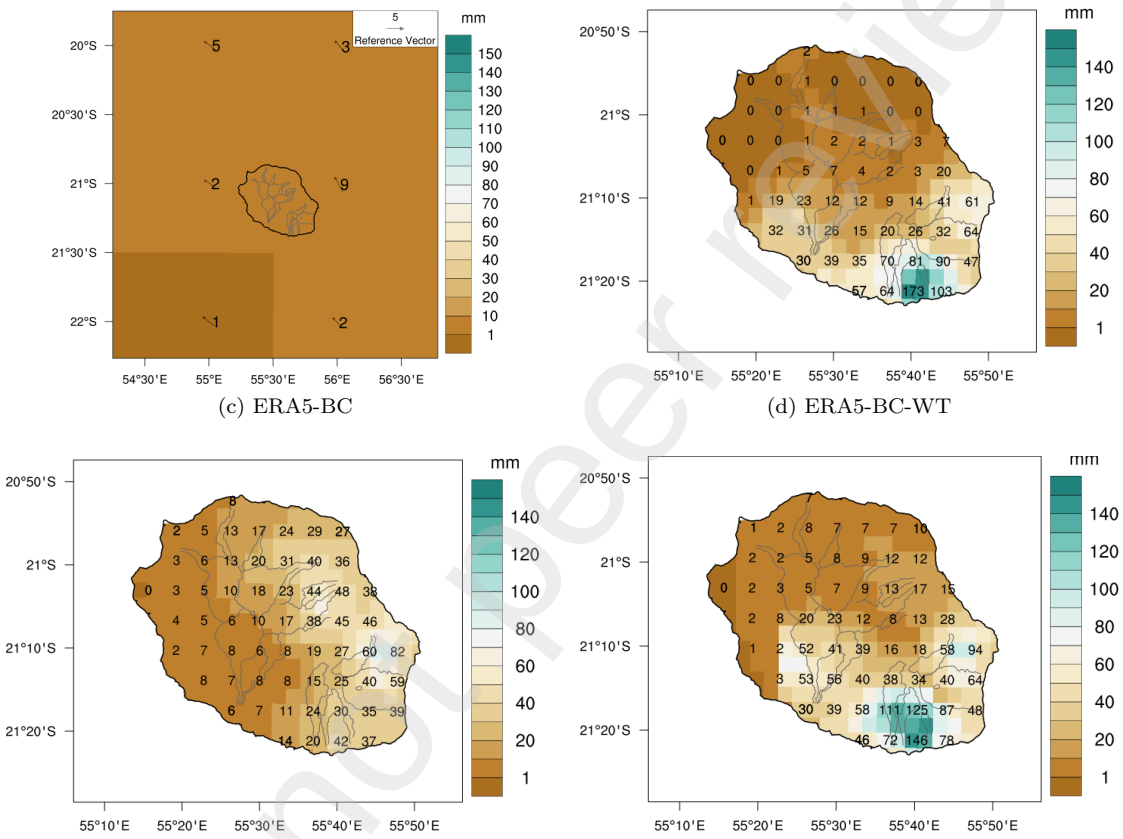

(c) ERA5-BC

(d) ERA5-BC-WT

Figure 3: Daily precipitation (mm, shaded) over La Réunion in a trough situation occurring on 1 May 2000 in (**a**) ERA5 degraded at 1° resolution, (**b**) observation krigged at 0.03° resolution, (**c**) ERA5 after simple bias correction (BC) at 0.03° resolution and (**d**) ERA5 after bias correction at 0.03° resolution using weather types (BC-WT). The arrows in (**a**) represent the direction and intensity of the ERA5 wind at 850 hPa. The size of the arrows is proportional to the wind intensity, with a reference arrow corresponding to a 5 m/s wind. Precipitation values are displayed on regular grid points.

(a) TRAIN (1981-2010) (b) TEST (2011-2017)

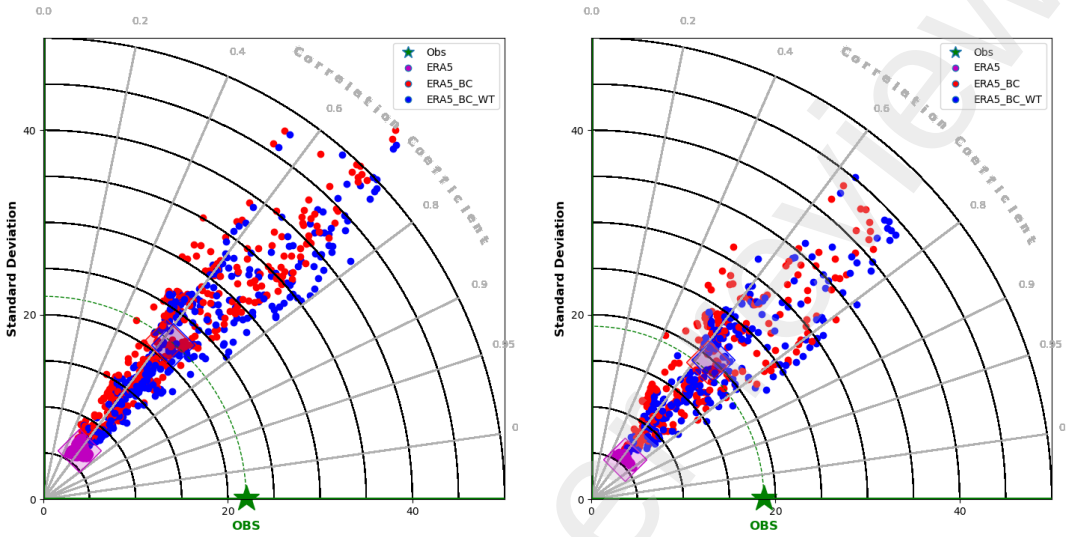

Figure 4: Taylor diagram for the (**a**) TRAIN (1981-2010) and (**b**) TEST (2011-2017) daily precipitation dataset at 0.03° obtained for different models: ERA5 interpolated at 0.03° resolution (in purple), ERA5 after simple bias correction (BC) at 0.03° resolution (in red) and ERA5 after bias correction at 0.03° resolution using weather types (BC-WT, in blue). Observations are in green. Dots represent the data on grid points and squares represent the mean over all grid points.

period (Fig. 4b). In conclusion, both ERA5-BC and ERA5-BC-WT successfully correct the large biases present in the ERA5 model, but ERA5-BC-WT demonstrates slightly superior performance overall.

Examining scores in individual wind sectors also reveals insights. In northerly winds, associated with extreme cyclonic events and heavy rainfall, RMSE and MAE values are higher, both in the TRAIN and TEST dataset. The bias correction method on ERA5 struggles to capture extreme weather conditions over the hills (circus and volcano area) when winds blow

from the North. This is due to the underestimation of heavy precipitation events in the ERA5 reanalysis (Appendix D). This issue may also occur for the CMIP6 models, impacting the performance of ERA5-BC-WT. This highlights the need for an improved approach for this regime or for a better representation of extreme precipitation events in ERA5 or GCMs. However, the statistical downscaling method is robust in capturing climate change signals for the quarters AMJ, JAS, and OND and compares well with the dynamical downscaling approach (see Appendix E).

4.2. Evaluation of CNRM-ESM2-1 and CNRM-ALADIN in a present-day climate

Both CNRM-ESM2-1 and CNRM-ALADIN models generally capture the SWIO's precipitation climatology well compared to IMERG and ERA5 reference datasets (Fig.5). They offer reasonable representations of the intertropical convergence zone and associated precipitation, but discrepancies are observed. CNRM-ALADIN, and to a lesser extent CNRM-ESM2-1, exhibit increased precipitation in the Chagos area (located near 5°S - 72°E) - a tropical cyclogenesis area - and a slight westward ITCZ extension. Both models also show more precipitation on the east coast of Madagascar and other windward coasts (see Fig.5).

Evaluating these discrepancies against ERA5 and IMERG faces challenges due to limited observational data coverage over the ocean, particularly during intense precipitation events like tropical cyclones [56, 73, 3]. Figure 5 highlights differences between ERA5 and IMERG, with ERA5 showing more precipitation on the east coast of Madagascar, possibly due to rain gauge assimilation, but lower levels within the ITCZ region over the sea. Evaluations

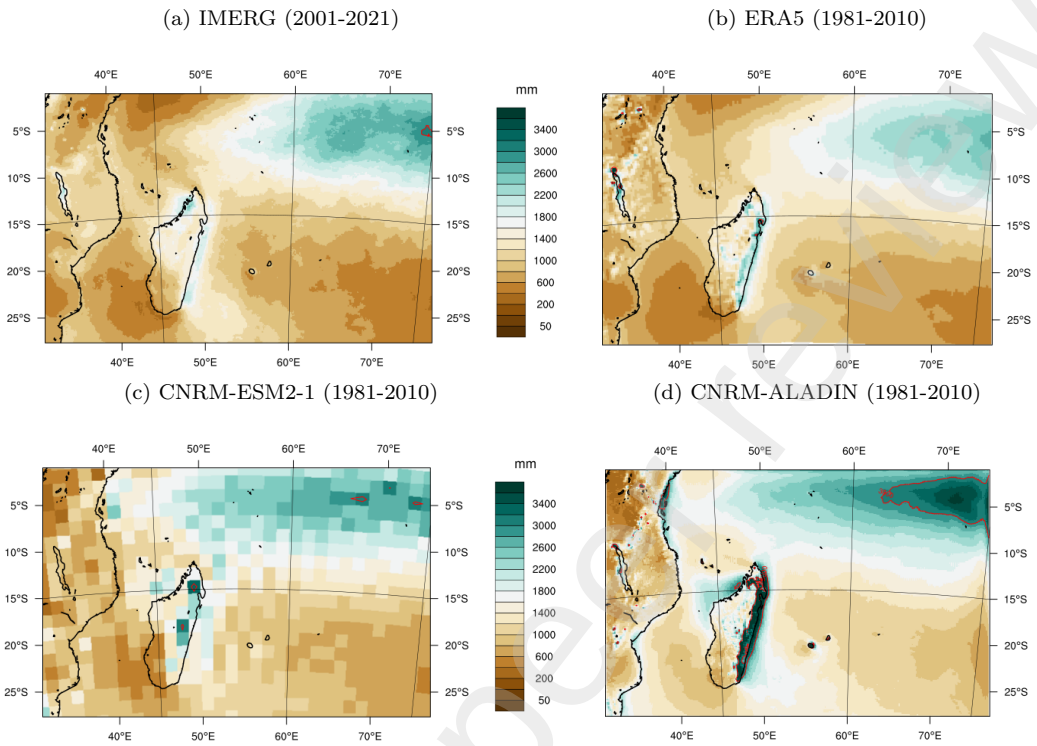

Figure 5: Average annual precipitation (mm) over the SWIO for (**a**) IMERG, (**b**) ERA5, (**a**) CNRM-ESM2-1 and (**d**) CNRM-ALADIN. Annul precipitation is averaged over time periods indicated in the subtitles of each panel. Red contours indicate precipitation greater than 3000 mm.

of ERA5 and IMERG in insular contexts like La Réunion, where high-quality in-situ observations are available, reveal significant underestimation of rainfall over steep terrain and along windward coasts (see Appendix D). On another hand, the CNRM-ALADIN model's internal characteristics could contribute to overly intense cyclones or overestimated precipitation in areas with significant terrain in trade wind regimes.

With a 12 km resolution, the CNRM-ALADIN model provides a partial representation of La Réunion's steep terrain. The real island, measuring ap-

proximately 75 km (from the northwest to the southeast) by 55 km (from the northeast to the southwest), features rugged topography, including a volcanic region with elevations of 2000 to 2600 meters (depicted at 1423 m in CNRM-ALADIN) and the towering 'Piton des Neiges' massif at 3070 meters (1460 m in CNRM-ALADIN). Despite orographic imperfections, the model effectively captures La Réunion's annual precipitation climatology, showing an east-west (windward-leeward) contrast and values approaching 11 meters in the highlands of Sainte Rose, consistent with observed maximum precipitation (Fig. D.19c). However, CNRM-ALADIN tends to overestimate precipitation on the west coast due to an overly elevated representation of orography. This limitation is addressed through bias corrections: applying the CDF-t method, the precipitation climatology in CNRM-ALADIN (Fig. D.19d) closely aligns with the observed 0.03° gridded climatology (Fig. A.15).

4.3. Position of CNRM-ESM2-1 and CNRM-ALADIN among CMIP6 Models

Figure 6 presents 21st century projections over the SWIO region under the SSP5-8.5 scenario using 22 CMIP6 models, some CMIP5 models, and the regional simulation CNRM-ALADIN. CNRM-ESM2-1 shows intermediate warming anomalies (with its low TCR of 1.86°C but quite high ECS of 4.76°C [63]) and significant decreases in annual precipitation (Fig. 6). CMIP5 models depict less warming and a balanced precipitation trend, while CMIP6 models mainly project a decline in precipitation under this high-emission scenario (Figs. 6, 7b). For other scenarios, SSP1-2.6 and SSP2-4.5, CMIP6 models show a lighter drying trend (not illustrated).

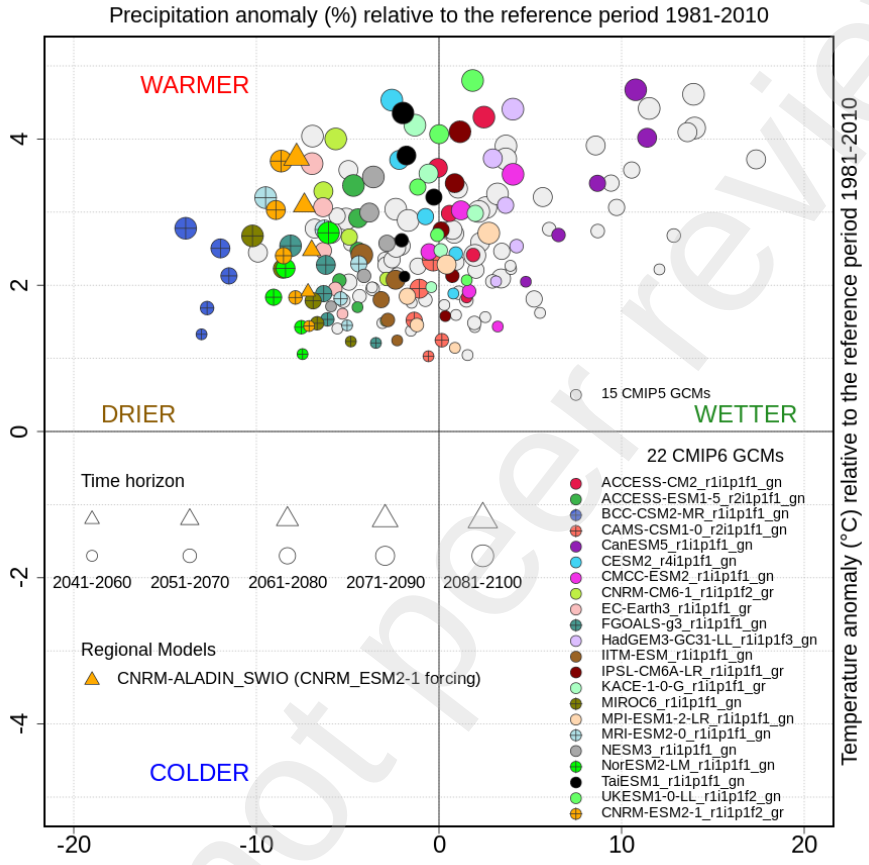

Figure 6: Anomalies in precipitation (x-axis) and temperature (y-axis) relative to the 1981-2010 reference period, expressed as percentages. Data is derived from the regional model (represented by orange triangles), a subset of 22 CMIP6 models (colored circles, with CNRM-ESM2-1 highlighted in orange) and 15 CMIP5 models (grey circles), all under the SSP5-8.5 scenario. The data, averaged within a designated box covering the Southwest Indian Ocean basin (34°-74°E ; 2-28°S), spans 20-year intervals and covers time horizons from 2050 to 2090 (symbol size increases with the time horizon). Plus symbols denote a subset of 7 CMIP6 models characterized by low ECS or low TCR values.

4.4. Future precipitation trends over the SWIO from CMIP6 models

The 22 CMIP6 models were regridded to a 2.5 latitude-longitude grid. A significant part of the southern tropics in the SWIO is projected to experience drying by the end of the century during the second semester in the SSP5-8.5 scenario (Figs. 7e, 7f), particularly in the dry trimester of July-August-September (Fig. 7e). The precipitation decline in October-November-December is associated with a delayed onset of the rainy season (Fig. 7f). The decrease in annual precipitation is more pronounced in the SSP5-8.5 scenario (Fig. 7b) compared to the SSP1-2.6 scenario (Fig. 7a, quarters not shown). Under the SSP5-8.5 scenario, over 90% of the CMIP6 models agree on an annual precipitation decline in a southern zone located east of Madagascar and along the southeast coast of Africa by the end of the century (Fig. 7b). Conversely, during the JFM trimester, an increase in precipitation is anticipated by the majority of models over part of the ITCZ, possibly linked to the strengthening of the monsoon trough (Fig. 7c).

4.5. Future evolution of tropical system activity

CNRM-ALADIN, with a 12-km resolution, can simulate Category 4 and 5 tropical cyclones and reproduces the climatology of tropical systems better than its parent model, CNRM-ESM2-1. It produces about half the annual number of tropical systems compared to the BT dataset confined to the same geographical domain. The model has a positive bias in the intensity of tropical systems, possibly due to lack of ocean coupling or weaknesses in physical parameterizations. After intensity calibration, the model's climatology aligns more closely with the BT dataset in terms of intensity distribution with similar ratios of systems per category.

(a) SSP1-2.6 AN

(b) SSP5-8.5 AN

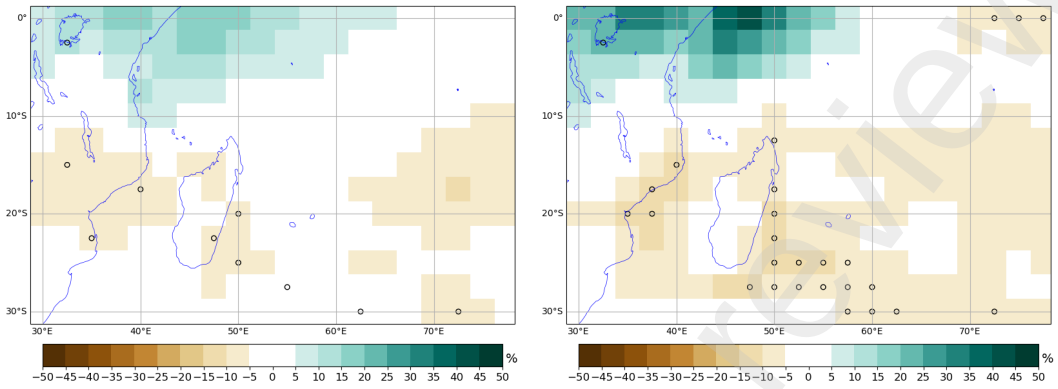

(c) SSP5-8.5 JFM

(d) SSP5-8.5 AMJ

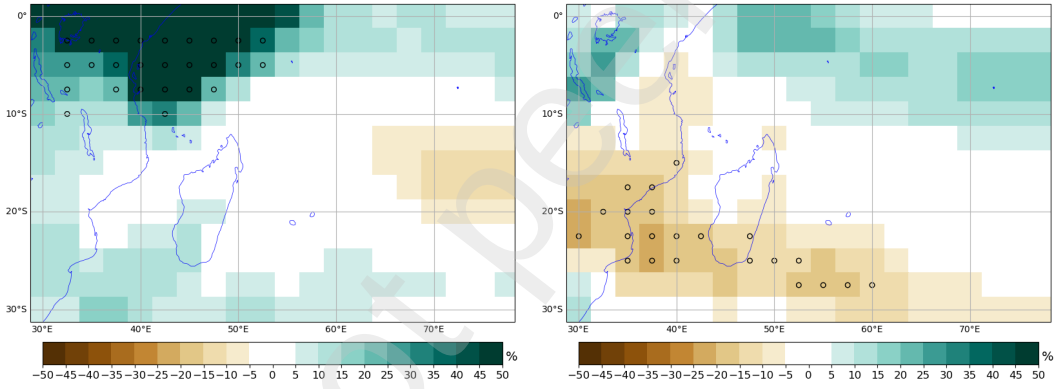

(e) SSP5-8.5 JAS

(f) SSP5-8.5 OND

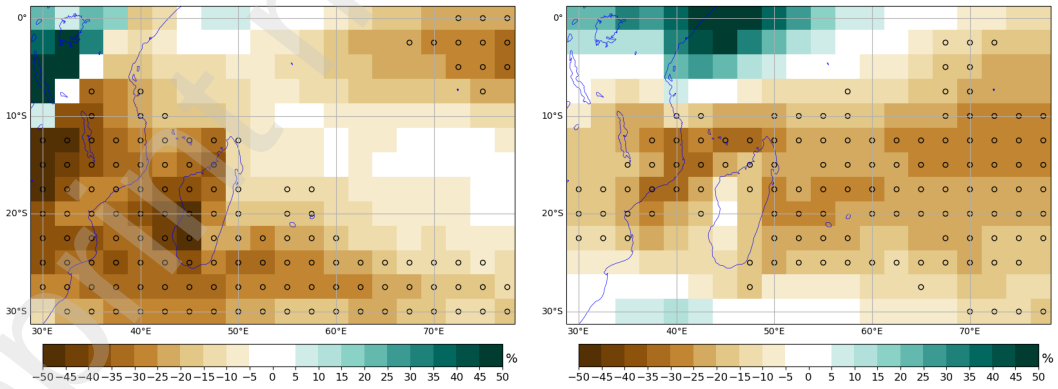

Figure 7: Precipitation Anomalies (in %, shaded) relative to the 1981-2010 reference period over the SWIO basin projected for the end of the century under various scenarios and time frames (annual or quarterly). These projections are averaged across 22 CMIP6 models. The scenarios and time periods include: (**a**) SSP1-2.6 for the year, (**b**) SSP5-8.5 for the year, and SSP5-8.5 for the quarters (**c**) JFM, (**d**) AMJ, (**e**) JAS, and (**f**) OND. Precipitations values are averaged over the 2060-2100 period. Brown shading indicates the driest areas, while blue represents the wettest. Circles mark grid points where more than 90% of the models agree on the sign of the anomaly.

In the future, CNRM-ALADIN predicts a reduction in the frequency of tropical systems, with an average decrease of 28% across all global warming levels (GWLs), consistent with the figures reported with a high-resolution model [a 20% decrease in a 2°C warmer world, 14]. This decline becomes more pronounced as global warming intensifies. The model shows that the proportion of intense cyclones is progressively increasing at the expense of weaker systems (Fig. 8), reflecting the anticipated response of tropical cyclones to global warming conditions. At a +4.0°C GWL, the maximum lifetime intensity of tropical cyclones in CNRM-ALADIN is expected to increase by a factor of 1.2 in terms of wind speed. The model forecasts a 30% increase in category 4–5 TC frequency (VITC, VMAX > 115 kts) at a +2.0°C GWL, and a 40% increase at +4.0°C. The proportion of 4–5 TC systems relative to all tropical storms (VMAX > 34 kts) is projected to double for the +4.0°C GWL and increase by approximately 1.5 times for lower GWLs in CNRM-ALADIN. The projected increase in category 4–5 proportion is directly correlated with the level of global warming. An increase in the duration of modeled tropical storms (VMAX > 34 kts) is also predicted as global warming progresses.

As a result, the average accumulated cyclone energy (ACE) per storm is expected to increase by about 36% for a +2.0°C GWL and 49% for a +4.0°C GWL, compared to the modeled historical average of 8.3 ACE units (10^4 kts^2). However, the evolution of seasonally integrated cyclone risk over a major portion of the SWIO basin (the domain of CNRM-ALADIN) is less dramatic. The average annual ACE for a +1.5°C GWL is expected to increase by about 14% compared to the modeled historical average of 30.6 ACE units

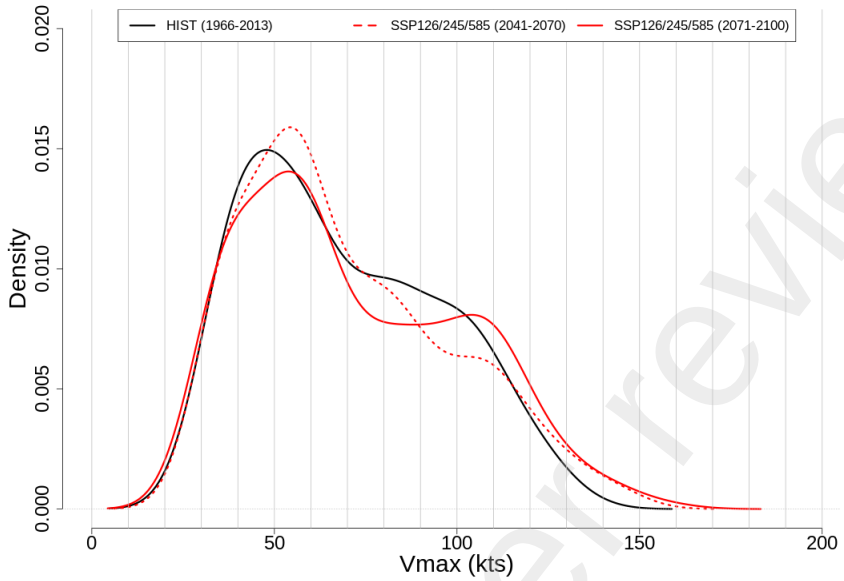

Figure 8: Evolution of the probability distribution function of the maximum wind speed of tropical systems in CNRM-ALADIN averaged across the three SSP scenarios. The historical reference period is shown in black, the mid-century horizon in dashed red lines, and the end-of-century horizon in solid red lines.

(10^4 kts^2) per year, but for a +2.0°C (+4.0°C) GWL, it shall decrease by about 4% (11%). The decline predicted for GWLs above +2.0°C is linked to the decrease in the number of tropical systems. Our regional projections also show that the most intense cyclones may occur at more southern latitudes in the future (consistent with [14]), further increasing TC risk for the Mascarene Islands.

4.6. Future temperature anomalies in countries of the SWIO

Compared to the reference period 1981-2010, near-surface (2 m) air temperatures over the SWIO region are projected to increase by an average of +1.2°C by the end of the century under the SSP1-2.6 scenario, with an un-

certainty of ±0.5°C given by the 80% envelope of the 22 CMIP6 models (Fig. 9). Large land masses like Madagascar and Africa will see the greatest increases. Under the SSP5-8.5 scenario, an average increase of +4.4°C is expected on Madagascar, while small islands will see lower yet substantial warming of +3.1°C to +3.7°C, with an uncertainty of ±1.0°C. Rates of regional warming are stable under the low emission scenario (SSP1-2.6) but accelerate under the high emission scenario (SSP5-8.5).

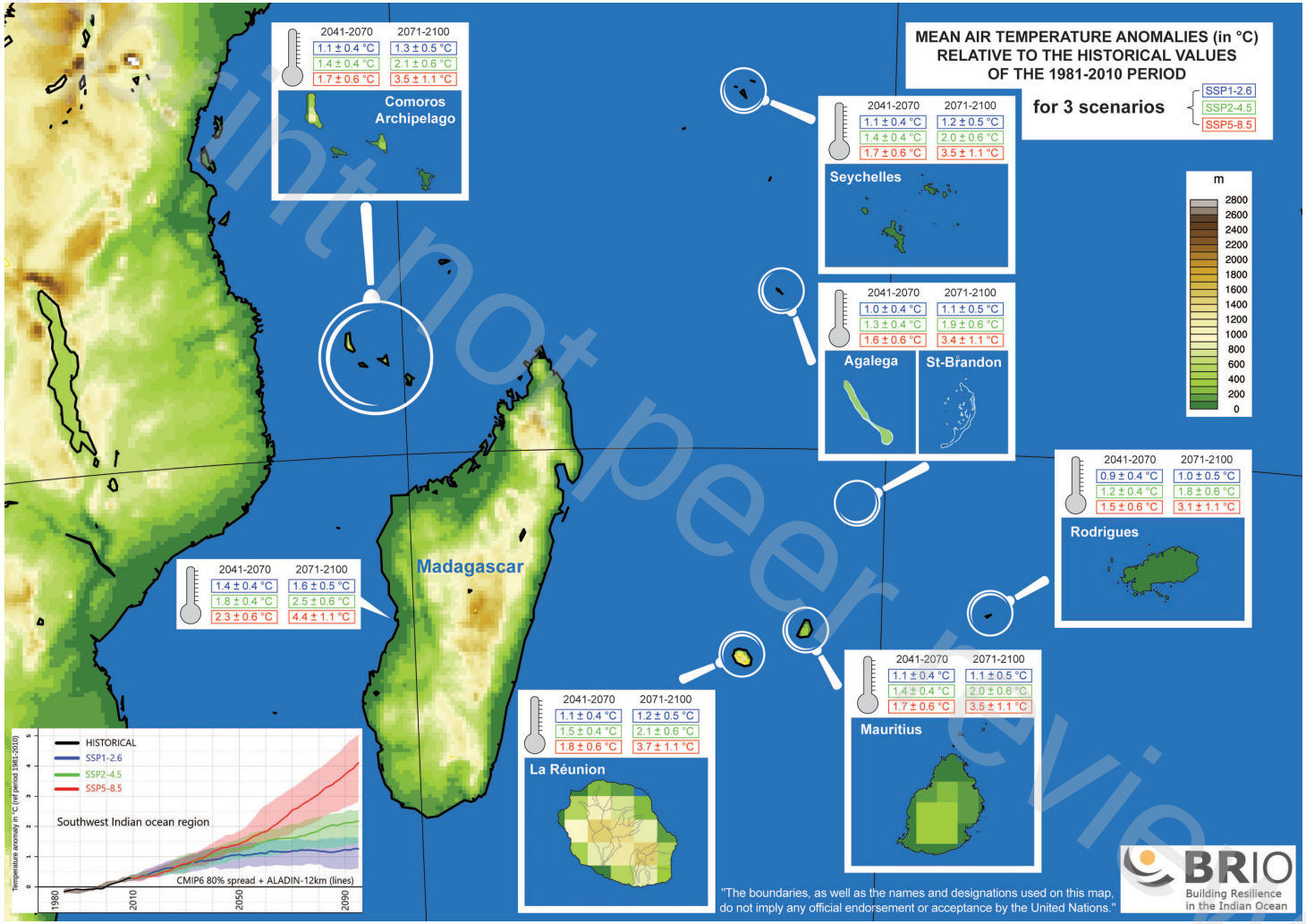

Figure 9: Near-surface (2 m) air temperature anomalies (in °C) relative to the reference period 1981-2010 derived from bias-corrected CNRM-ALADIN outputs under 3 SSP scenarios, represented by different colors, for the various IOC islands. The uncertainty ranges calculated using the 80% spread of temperatures anomalies from the 22 CMIP6 models are also indicated. The time series in the bottom left corner shows the evolution of temperature anomalies in the three SSP scenarios for CNRM-ALADIN (solid lines) and for the subset of 22 CMIP6 models (80% confidence interval envelopes). The background map represents the orography in CNRM-ALADIN.

4.7. Future precipitation trends in cities of the SWIO

The dry season (June-November) in the tropical to subtropical part of the southwest Indian Ocean is projected to become significantly drier, with precipitation deficits of 10% to 40% (Fig. 10). This is due to a delayed onset of the rainy season (starting in December instead of November) and a stronger or more persistent Mascarene anticyclone, especially under the SSP5-8.5 scenario (not illustrated). This drying trend is more pronounced as global warming intensifies. The strengthening of subtropical high-pressure systems is expected to accelerate the trade winds over the Mascarene Islands, particularly during winter, when the trade winds already blow forcefully. Over La Réunion, the topography will modulate these values through acceleration effects on the northern and southern coasts of the island. In conclusion, more intense or frequent trade wind episodes can be anticipated in the future, especially in the high-emission scenario.

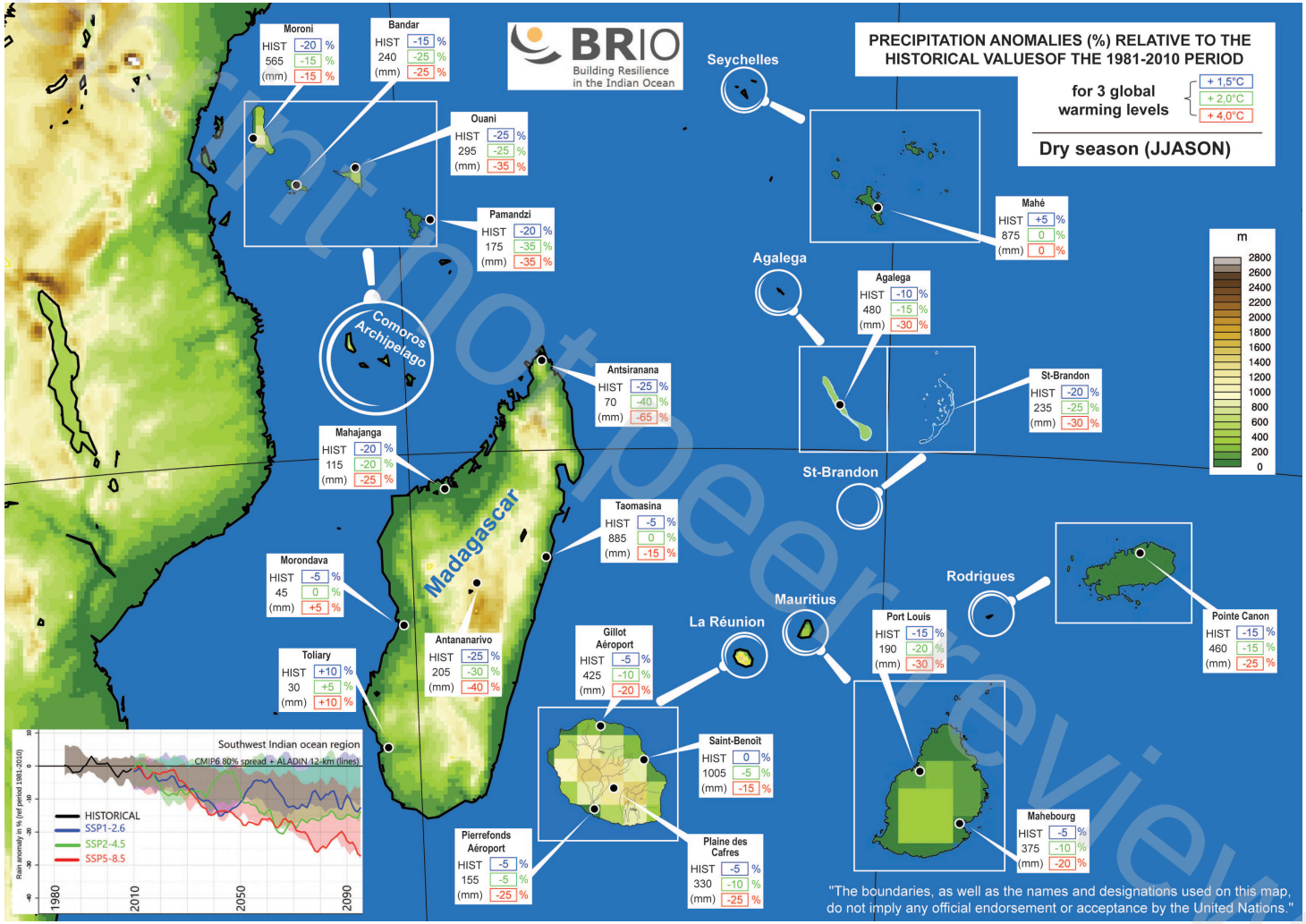

Figure 10: Precipitation anomalies (in %) relative to the reference period 1981-2010 during the dry season (From June to November) derived from bias-corrected CNRM-ALADIN outputs. Displayed are the expected precipitation anomalies for various cities in IOC countries under three global warming levels, represented by different colors. The values of cumulative precipitation during the reference period (mm) are also indicated. The time series in the bottom left corner shows an evolution of wet season precipitation anomalies averaged over the SWIO basin under the three SSP scenarios for CNRM-ALADIN (solid lines) and for the subset of 22 CMIP6 models (80% confidence interval envelopes).

Figure 11 shows precipitation trends during the wet season (December-May) under three global warming levels. Most cities in the SWIO region, except Rodrigues, St Brandon, and Toliary (located southwest of Madagascar), are projected to have reduced precipitation according to CNRM-ALADIN. However, these projections have a high level of uncertainty, ranging from $\pm 5\%$ to $\pm 10\%$.

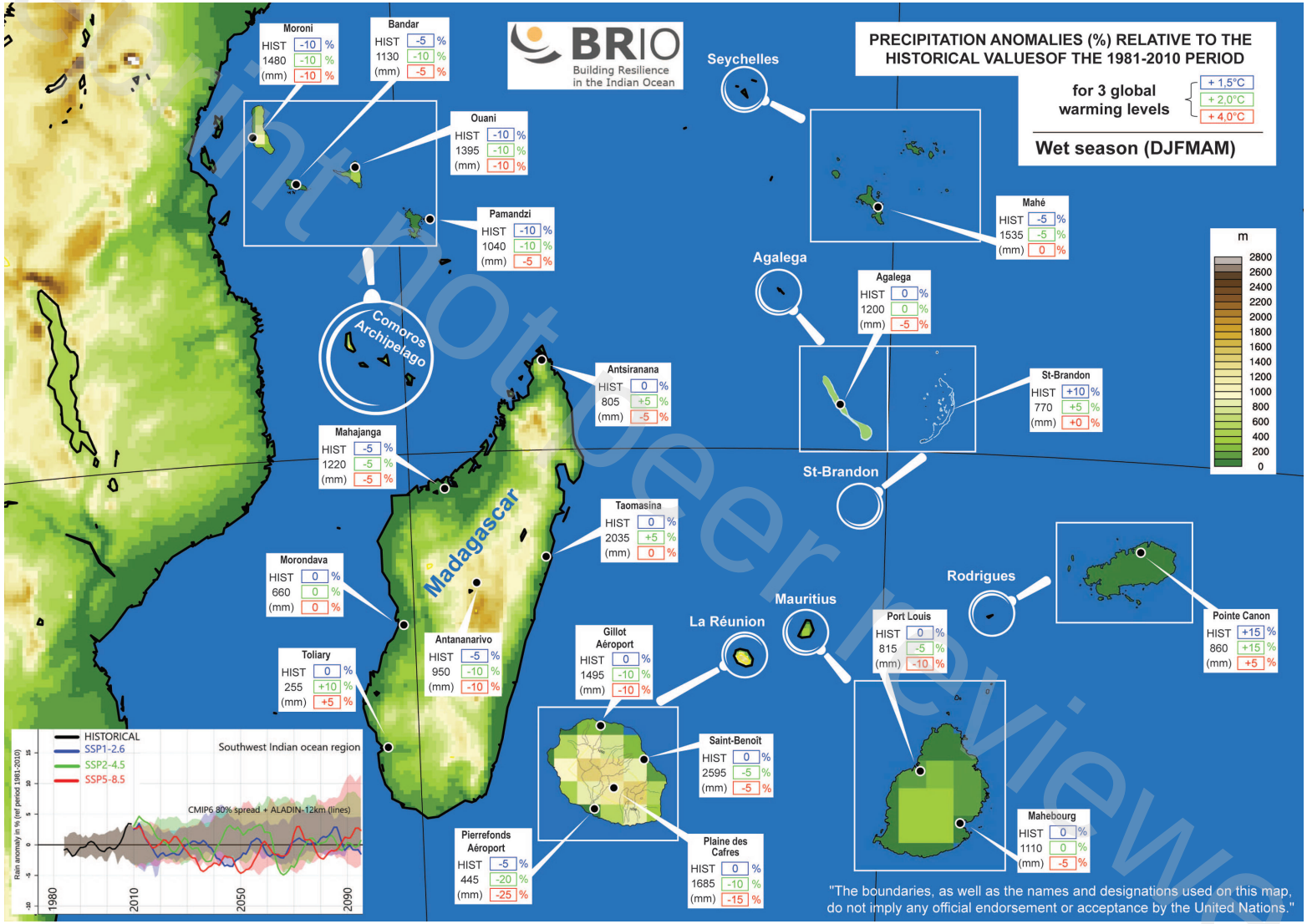

Figure 11: As in Fig. 10 but for the wet season (From December to May).

4.8. Heat waves and extreme temperatures in St Denis

CNRM-ALADIN results show more pronounced warming on the minimum temperatures (TN) along La Réunion's west coast, while the most significant rise of maximum temperatures (TX) is expected in the highlands and interior. The mean temperature increase varies across the island, gradually increasing with altitude from the coast to the center (Fig. 4 of [44]). Warming differences between the coast and center range from 0.2°C in the SSP1-2.6 scenario to 0.8°C in the SSP5-8.5 scenario. It's during the peak of the hot season (JFM) that temperatures will experience the most substantial increase (not shown), with the likelihood of extreme heat episodes particularly impacting coastal areas.

Gillot, situated on La Réunion's north coast near Saint Denis, may experience temperatures comparable to those in Pamandzi, Mayotte, by the end of the century under the SSP5-8.5 scenario. Historical daily mean temperatures averaged 23.6°C in Gillot and 26.7°C in Pamandzi over the 1985-2014 period in CNRM-ALADIN. In the SSP5-8.5 scenario, Gillot's average daily mean temperature is projected to align with Pamandzi's historical average around 2070-2090. Maximum temperatures in Gillot could potentially reach as high as 44.5°C under this worst-case scenario.

Figure 12 illustrates the evolution of heatwaves in Gillot under two extreme scenarios: SSP1-2.6 (in blue) and SSP5-8.5 (in red). The average daily mean temperatures are examined to compute thresholds on a 30-year historical period centered on year 2000. For Gillot, a heatwave is detected when the average temperature exceeds 27.9°C (99.5^{th} percentile of the historical distribution). The adjacent days to this peak, for which the average temperature

remains above 27.3°C (97.5^{th} percentile) for at least 3 consecutive days, are included in the episode. An episode concludes when the temperature falls below 26.9°C (95^{th} percentile). In Figure 12, the size of each bubble, showing a heatwave event, reflects the severity of the heatwave, which is proportional to the cumulative heat during the episode (it is computed as the integral area under the curve above the 97.5^{th} percentile). The horizontal position shows the duration (in days) of the episode, while the vertical position displays the intensity, representing the maximum daily mean temperature reached during the episode.

Each year won't necessarily be hotter than the previous one due to natural fluctuations (Fig. 12). However, over the long term, heatwaves will increase in duration, severity, and intensity, with daily mean temperatures reaching up to 35.5°C in Gillot under the high-emission scenario. The increase in heatwaves will be less pronounced in the SSP1-2.6 scenario than in the SSP5-8.5 scenario, emphasizing the need for climate change mitigation. In all cases, the increase in heatwaves will be significant compared to the historical period (barely visible in Figure 12), necessitating adaptation to their impacts.

The number of days with high temperatures is expected to significantly rise (Fig. 13). During the last decade (2011-2020), the recorded maximum temperatures have already exceeded the 31°C threshold for an average of 38 days per year in Gillot, with a peak of 103 days in 2019 (black dots in Fig. 13). The 2019 year was notable for its elevated sea surface temperatures around La Réunion, attributed to an El Niño-like event and a positive Indian Ocean Dipole. By the end of the century, the maximum temperature will exceed 31°C at Gillot half of the year if no action is taken to reduce global greenhouse

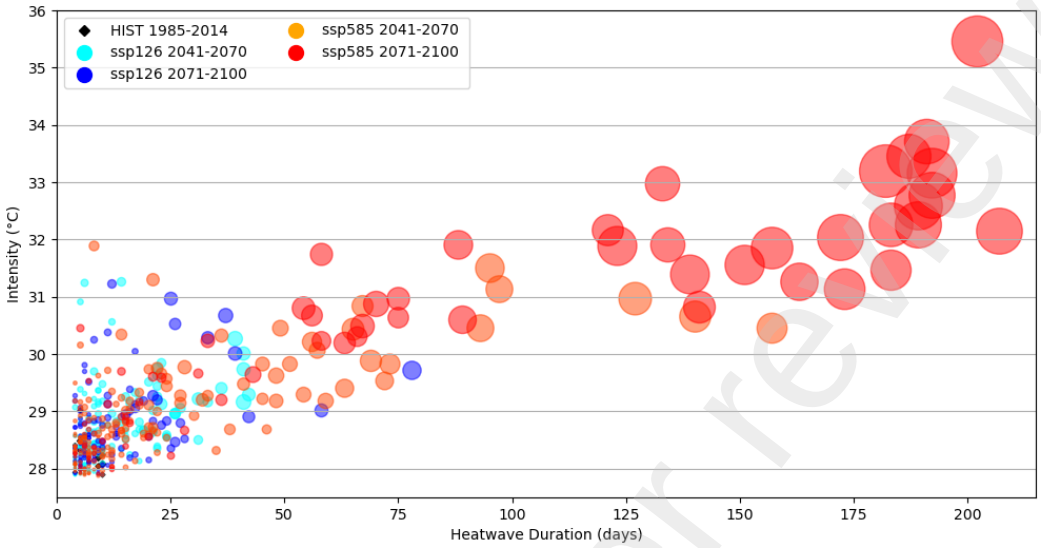

Figure 12: Heatwaves over Gillot (La Réunion) from 1981 to 2100 for two SSP scenarios computed from CNRM-ALADIN bias corrected outputs. Thresholds for heatwave identification are defined using the 1985-2014 period.

gas emissions. It shall be multiplied by 3 under scenario SSP1-2.6 compared to the modeled mean historical value of 13 over the 1981-2014 period. The trend of days exceeding the 31°C threshold is higher for CNRM-ALADIN than for the mean of 22 CMIP6 models under the SSP5-8.5 scenario after 2070. A slightly more optimistic trend is given by the subset of 7 CMIP6 models with low ECS or low TCR values (solid envelopes in Fig. 13).

4.9. Future precipitation trends over La Réunion

Figure 14 shows median projected precipitation anomalies during the dry season for the SSP1-2.6 and SSP5-8.5 scenarios in the mid and late 21st century, derived from statistically downscaling 22 CMIP6 models over La Réunion. December is included in the dry season due to future delays in the

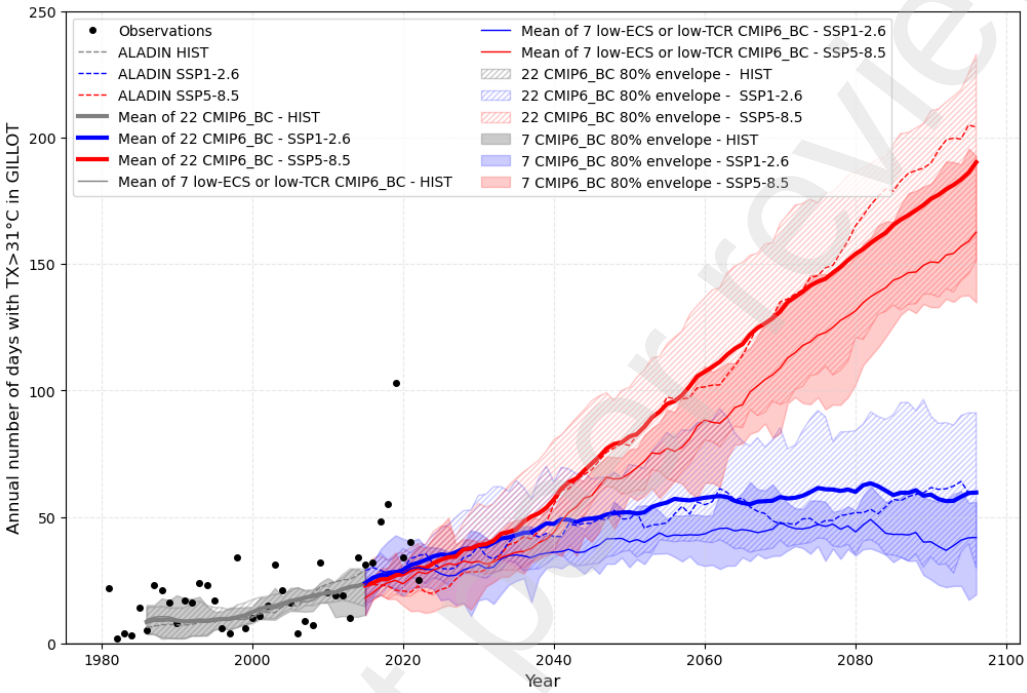

Figure 13: Temporal evolution of the annual count of days with temperatures surpassing the 31°C threshold at Gillot for the SSP1-2.6 (in blue) and the SSP5-8.5 (in red) scenarios over the 1981-2100 period. A rolling mean with a 10-year window is applied on each model data before computing quantiles and means. Dashed lines represent outputs from the regional model. Bold (light) solid lines denote the mean of the warming projected by 22 CMIP6 models (specifically, a subset of 7 models characterized by low ECS or low TCR values) after applying statistical downscaling. The hatched (solid) envelopes encompass the 80% confidence interval generated from the 22 CMIP6 models (specifically, the subset of 7 low-ECS or low-TCR models). Observations for each individual year within the 1981-2022 period are depicted as black dots.

rainy season onset. CNRM-ALADIN provides similar values to the median of the CMIP6 models (see Appendix F). Trends show a greater reduction in precipitation as global warming intensifies, with an east-west contrast. Precipitation decreases are most pronounced on the western (leeward) side of the island, while the decline is less significant along the eastern coast exposed to trade winds.

5. Discussion

In this article, we have described the projected changes in precipitation, temperatures, and cyclonic activity in the SWIO basin under various greenhouse gas emission scenarios and warming levels. We used a regional climate model capable of generating realistic cyclone simulations. To understand uncertainties in precipitation and temperature modeling, we analyzed 22 CMIP6 models. These models underwent statistical downscaling using weather types over La Réunion to produce data for climate services.

We have created climate datasets in a region overlooked by CORDEX domains. Our approach surpasses conventional frameworks like large CORDEX ensembles by international communities. We used an extended domain and higher resolution than CORDEX, providing a more accurate representation of tropical system climatology and precipitation across many small islands.

However, our approach has limitations. One is the use of a unique combination of regional (RCM) and global (GCM) models for high-resolution experiments. To address this, we compared the trends observed in our models with other CMIP6 models to establish the relative position of our GCM-RCM storyline. Considering the temperature and precipitation variations among

(a) SSP1-2.6 2041-2070

(b) SSP1-2.6 2071-2100

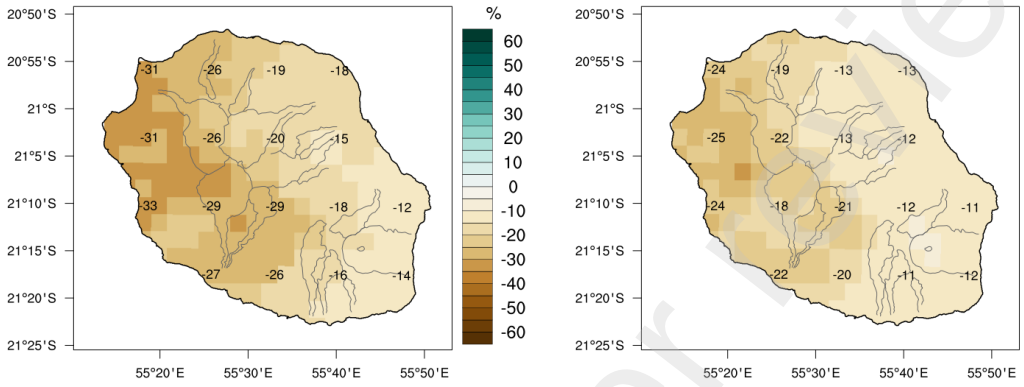

(c) SSP5-8.5 2041-2070

(d) SSP5-8.5 2071-2100

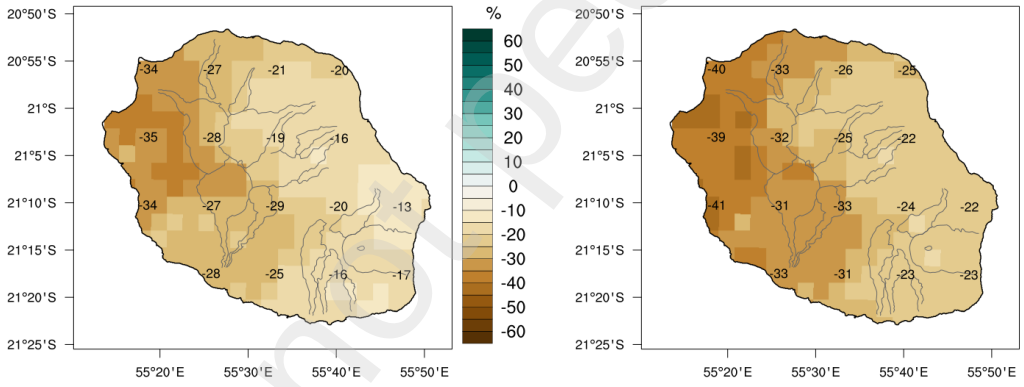

Figure 14: Median (Q50) of precipitation anomalies (%) during the extended dry season (June to December) derived from 22 CMIP6 models after applying statistical downscaling using weather types (BC-WT) at a 0.03° resolution. Displayed are the precipitation anomalies during the dry season (From June to November) in the SSP1-2.6 (row 1) and SSP5-8.5 (row 2) scenarios for the time horizons 2041-2070 (left column) and 2071-2100 (right column) relative to the 1981-2010 reference period. The color palette indicates the magnitude of anomalies.

the 22 CMIP6 models (Fig. 6), IPSL-CM6A-LR or UKESM1-0-LL, along with ACCESS-ESM1-5, could be interesting storylines for downscaling with CNRM-ALADIN or another regional model. This would provide additional GCM-RCM combinations to sample uncertainties over the SWIO region. We are also considering implementing a statistical emulator of our regional climate model such as [22]. This approach involves training neural networks to learn the downscaling function between large-scale atmospheric parameters and small-scale surface variables daily. If successful in our tropical region, it could provide a cost-effective way to generate downscaled climate projections from other CMIP6 models.

Another limitation in our study is the overestimation of cyclone intensities in CNRM-ALADIN, potentially due to the absence of ocean feedback or to the convection parameterization. Using a convection-permitted model like CNRM-AROME [10, 48] at 2.5 km resolution could provide a more accurate representation of extreme events, such as tropical cyclones and heavy rainfall. Despite this, and after cyclone intensity bias correction, our results align quantitatively with other high-resolution modeling studies [e.g., 14], showing a decrease in tropical cyclone frequency with climate warming and confirming that this decreasing trend is not an artifact of low resolution [40].

Our regional climate model generally aligns with the median of the statistically downscaled CMIP6 models over La Réunion, except during the peak of the wet season (JFM) when deep convection is prevalent. CNRM-ALADIN tends to produce more precipitation over the island during this period, possibly for valid reasons. We have therefore chosen to avoid discussing extreme precipitation events.

The statistical downscaling method we used, based on weather regimes, was developed for an insular tropical context like La Réunion. It can be extended to other islands in the region, particularly those with complex terrain, such as Madagascar and Mauritius, provided that the wind regimes are tailored to local climate specificities. Its implementation can offer valuable insights into local-scale climate dynamics. However, it may struggle to accurately quantify heavy precipitation events. A multivariate quantile-mapping algorithm [13] or machine learning techniques could better manage these events.

6. Conclusions

Our study aimed to examine the impact of climate change on small SWIO islands (including SIDS) and Madagascar, and generate CMIP6-based datasets for climate services, using La Réunion as an example. We assessed climate change under three emission scenarios and various warming levels.

In situ rain gauges revealed limitations of ERA5 reanalysis and IMERG satellite data over tropical islands with complex terrain like La Réunion and Madagascar, which tend to underestimate rainfall. We used various methods to combine the CMIP6 ensemble with downscaling techniques to obtain fine-scale climate information over the SWIO basin:

- We consolidated reference datasets for the IOC islands.
- We downloaded daily datasets for temperature, precipitation, and wind at 850 hPa for 22 CMIP6 models over 1981-2100, classified them into two categories, and analyzed temperature and precipitation dispersion.

- We conducted 12-km resolution regional climate runs using CNRM-ALADIN driven by CNRM-ESM2-1 for 1981-2100 under three SSP scenarios across an extended SWIO domain encompassing all the inhabited territories of the southwest Indian Ocean.

- We corrected CNRM-ALADIN biases at station points or at 3 or 4-km resolution over the SWIO islands.

- We statistically downscaled 22 CMIP6 models over La Réunion to quantify uncertainties, using an innovative bias correction method based on wind sectors. This method can be extended to other islands in the region with steep orography.

Our framework, which integrates the CMIP6 ensemble with various downscaling methods, could serve as a model for other regions with limited CORDEX coverage.

The CNRM-ALADIN storyline represents a median or high-end scenario (in the low TCR GCMs subset) for temperature and exhibits relatively dry conditions. Our study reveals significant climate change impacts in the region:

- **Temperature Increase:** Average temperatures on small islands are projected to rise by 1.1 (SSP1-2.6) to 3.7°C (SSP5-8.6) by the century's end, with Madagascar potentially experiencing up to a 4.4°C average increase in the high-emission scenario (SSP5-8.5), relative to the reference period 1981-2010. The uncertainty ranges from ±0.5°C (SSP1-2.6) to ±1.1°C (SSP5-8.5).

- **Heat waves:** The frequency of hot days is expected to rise significantly. Gillot, located near Saint Denis on La Réunion, may experience temperatures comparable to current conditions in Pamandzi, Mayotte, by the end of the century. The average annual count of days exceeding 31°C at Gillot is projected to escalate from 13 in the model 1981-2014 period to 50 under scenario SSP1-2.6 or 180 under scenario SSP5-8.5 by the end of the century.

- **Regional Precipitation Changes:** CMIP6 models indicate a decline in annual precipitation across the southern zone east of Madagascar, with a more pronounced reduction as global warming intensifies. Over La Réunion, this reduction may average approximately -2% per degree of global warming in both dynamical and statistical downscaling approaches. Conversely, an increase in precipitation is anticipated during the first trimester of the year over the ITCZ. The regional climate simulation also shows an increase in the magnitude of wet and dry years.

- **Dry Season Intensification:** The dry season in the tropical to subtropical part of the southwest Indian Ocean is expected to become significantly drier, with deficits ranging from 10% to 40%, due to a delayed onset of the rainy season and a stronger or more persistent Mascarene anticyclone. More intense and longer drought episodes are expected over Madagascar, the Comoros Archipelago, and the Mascarene islands. In La Réunion, a more significant reduction in precipitation is anticipated on the western side (leeward), accentuating the historical east-west contrast associated with trade winds.

- **Cyclonic Risk Increase:** The frequency of tropical cyclones is expected to decrease as the climate warms, especially for weaker storms, with an average reduction of 28% across all global warming levels. However, the frequency of Category 4 and 5 storms (VMAX > 115 kts) in the SWIO region is projected to rise with ongoing warming, reaching +30% for a +2.0°C GWL and potentially up to +40% for a +4.0°C GWL. Simulations also indicate a rise in maximum TC intensities, by up to a factor of 1.2. The duration of tropical systems with VMAX > 34 kts is also expected to increase as global warming progresses. As a consequence, the average accumulated cyclone energy per storm is projected to rise by approximately 36% for a +2.0°C GWL and 49% for a +4.0°C GWL. However, the overall seasonally integrated cyclone risk across a significant portion of the SWIO basin is expected to decrease for a global warming greater than +2.0°C, due to the decline in the number of tropical systems. Simulations also indicate a poleward shift in the latitude of TC maximum lifetime intensity with ongoing climate warming. These findings imply higher cyclonic risks for islands such as the Mascarenes or Madagascar.

Projected climate changes in the region will significantly impact ecosystems, water resources, agriculture, public health, and economic development. These changes will render both populations and infrastructure increasingly susceptible to a range of climate-related challenges, including heatwaves, droughts, coastal flooding, and intensified cyclonic winds and waves.

Our research provides a comprehensive overview of anticipated regional climate shifts, emphasizing the need for greenhouse gas emission mitigation

and preparedness for climate change consequences. We have demonstrated the adaptability of CMIP6-derived climate information to address challenges in small and large, mountainous island regions. Our accessible BRIO dataset contributes to numerous impact studies on La Réunion. In conclusion, this study showcases effective information distillation in an information-scarce context and amidst limited resources, serving as a potential model for other vulnerable regions with limited CORDEX coverage. Future research will study heat stress risks in humid conditions.

Appendix A. Climatology of precipitation over La Réunion

La Réunion experiences highly variable precipitation, both in space and time. Rainfall can be substantial on the east coast, while the west coast may remain dry. Rainfall patterns can shift dramatically, with extended dry periods followed by heavy rainfall events. The island holds numerous global records for rainfall duration. Rainfall is lowest on the western (leeward) coast, averaging around 500 mm per year, but increases with elevation (Fig. A.15). The Takamaka region and the eastern flank of the volcano receive particularly heavy rainfall: 7 meters per year for Takamaka (7.2 m in the kriged dataset) and more than 10 m per year in the Highlands of Sainte-Rose (9615 mm in the kriged dataset), which is exceptional on a global scale (Fig. A.15). The leeward region experiences prolonged drought periods during the austral winter (over 300 days without precipitation in Le Port), whereas the windward region has better-distributed rainfall throughout the year (over 300 days of precipitation in Piton Sainte-Rose).

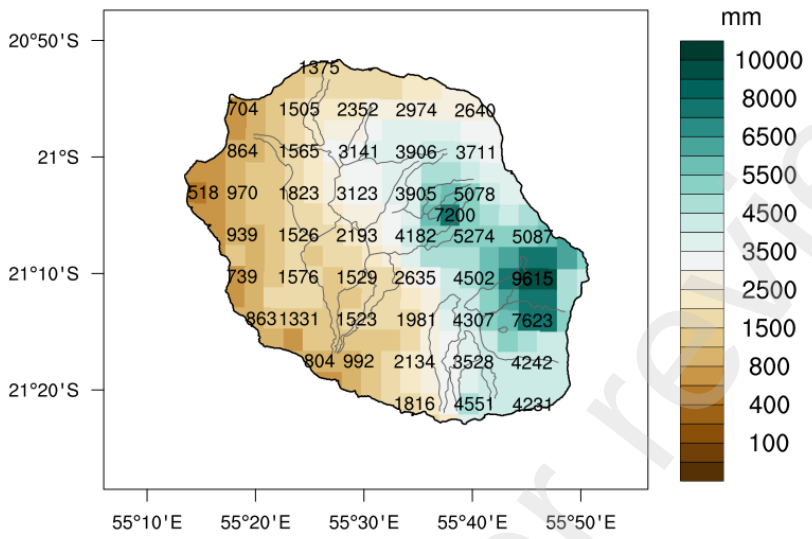

Figure A.15: Average annual precipitation (mm) over La Réunion in the kriged spatial observation product at 0.03° resolution over the 1981-2010 period.

Appendix B. Historical trends of precipitation over La Réunion and Mayotte

There hasn't been a notable historical trend in annual precipitation across La Réunion as a whole. However, over the past six decades, there has been a 36% decline in annual precipitation in the southwest region (Fig.B.16). Similarly, on Mayotte, dry-season precipitation (May to October) has decreased by 33% over the past 60 years (Fig.B.17).

Appendix C. Historical trends on the number of tropical systems in the SWIO

While there is no significant evolution in the number of tropical systems over the southwest Indian Ocean, both at the tropical storm and tropical

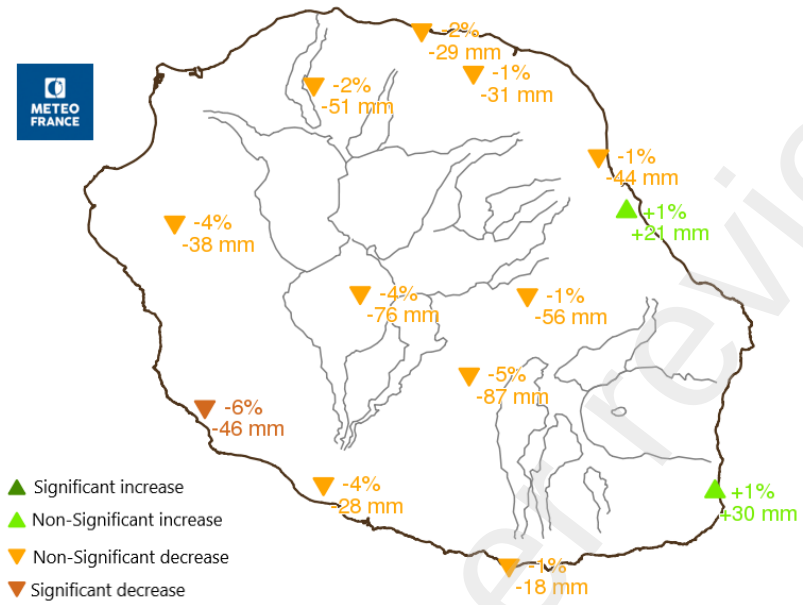

Figure B.16: Decadal precipitation trend calculated from annual precipitation measurements spanning 1961 to 2022 across multiple rain gauges in La Réunion.

cyclone stages, notable annual and decadal variability is evident over the past 41 years (Fig. C.18).

Appendix D. Evaluation of ERA5 and IMERG precipitation over La Réunion

Both ERA5 (Fig. D.19a) and IMERG (Fig. D.19b) data sketch out the west-east precipitation contrast over La Réunion. However, even with a finer 10-km resolution, IMERG does not accurately capture the spatially variable annual rainfall, nor does it accurately represent the high values associated with extreme precipitation events. Figure D.19 clearly illustrates rainfall underestimation in the reanalysis or satellite observation data over the steep terrain of a tropical island like La Réunion, especially along the windward

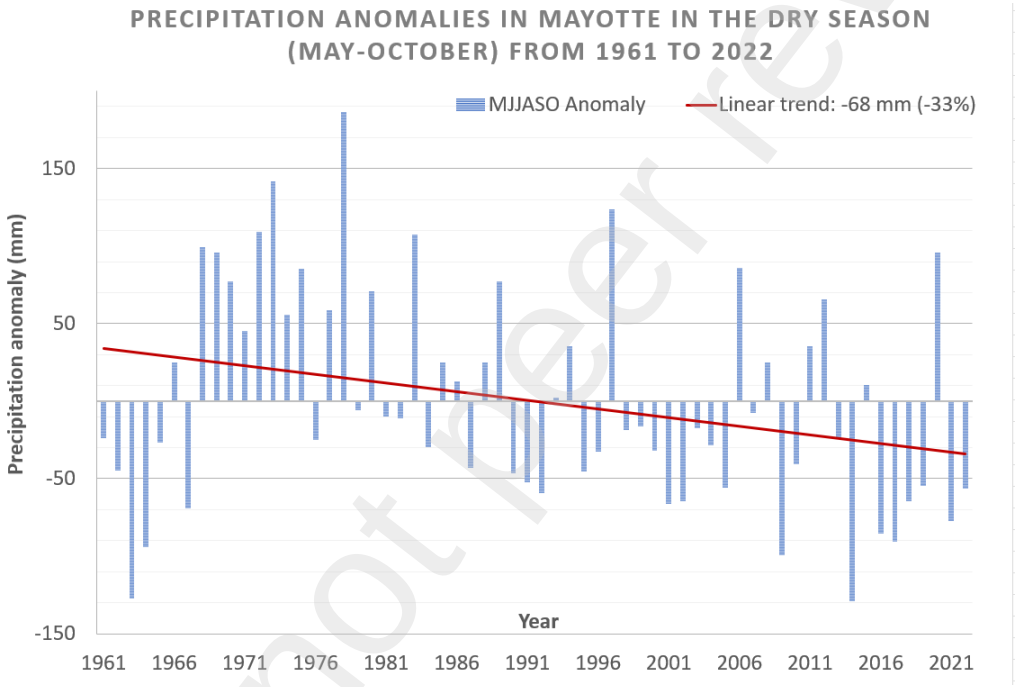

Figure B.17: Temporal evolution of observed precipitation anomalies from 1961 to 2022 during the dry season (May to October) over Mayotte, relative to the average value for the 1961-2022 period. Data from 2 rain gauges were used to compute the anomalies.

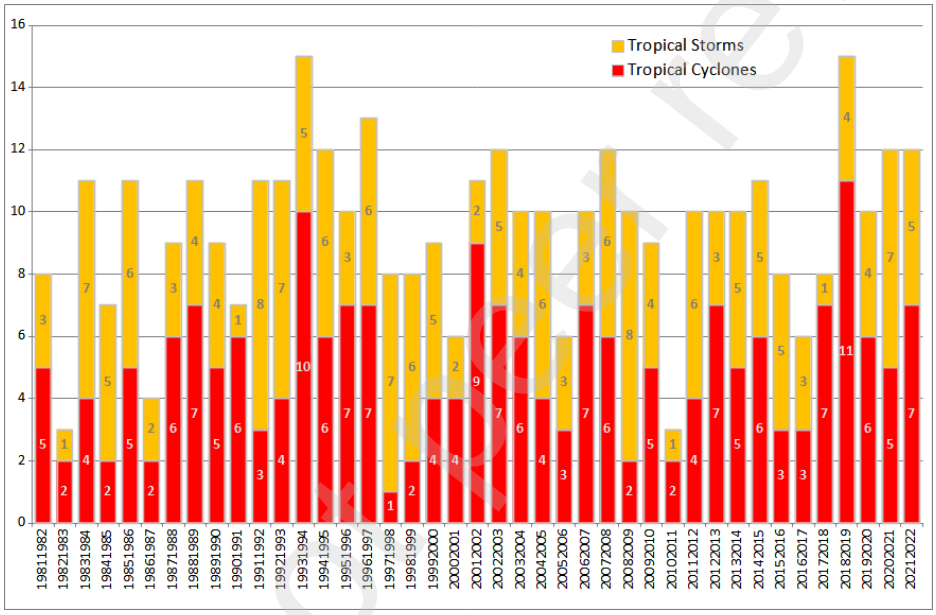

Figure C.18: Temporal evolution of the number of tropical storms (VMAX >= 34 kt) and tropical cyclones (VMAX >= 64 kt) in the southwest Indian Ocean, spanning from the 1981-1982 to the 2002-2003 tropical seasons, based on data recorded by RSMC La Réunion.

(east) coast. In the 1981-2010 period, the daily precipitation maximum is 1613 mm in observations and 202 mm in ERA5, which does not capture the precipitation maxima effectively.

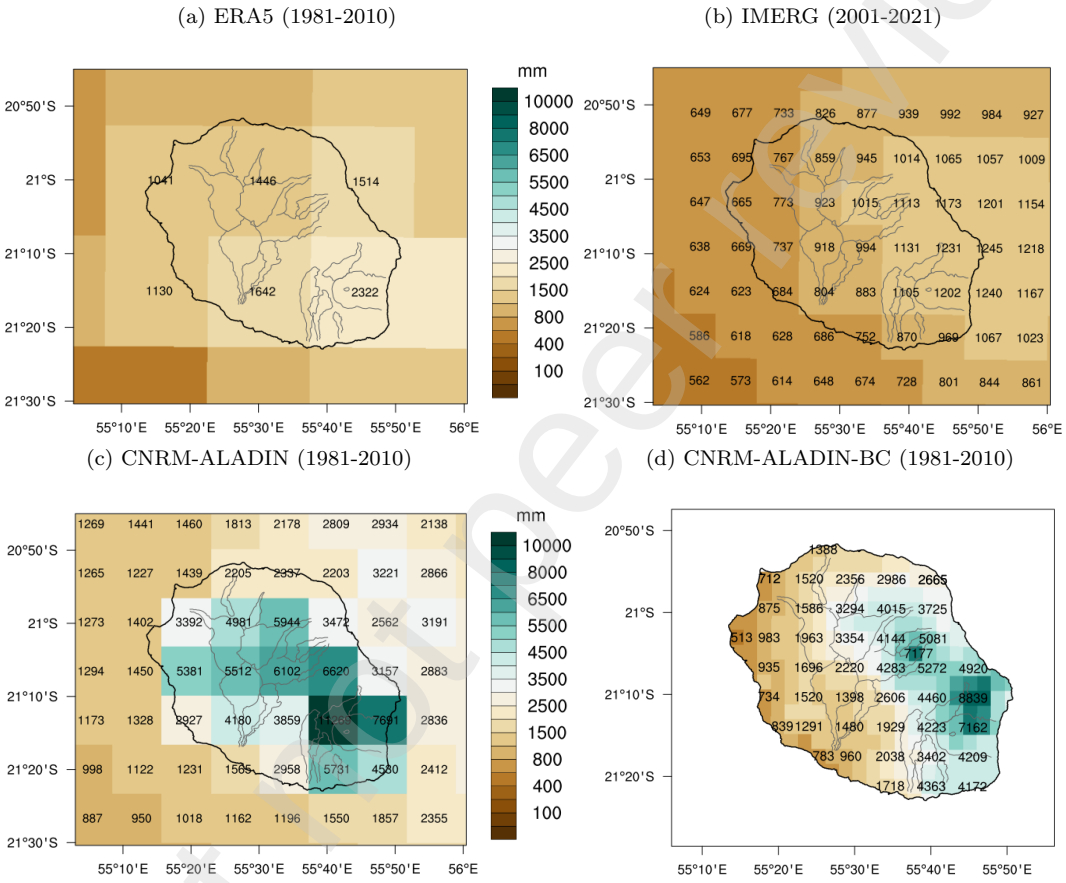

Figure D.19: Average annual precipitation (mm) over La Réunion in (**a**) ERA5, (**b**) IMERG, (**c**) CNRM-ALADIN at its native 12 km resolution, and in (**d**) CNRM-ALADIN after bias correction at 0.03° resolution. Annul precipitation is averaged over time periods indicated in the subtitles of each panel.

Appendix E. A comparison between statistical downscaling and dynamical downscaling

We compared the statistical downscaling of CNRM-ESM2-1 with the dynamical downscaling of CNRM-ALADIN for the SSP1-2.6 and SSP5-8.5 scenarios and various time horizons. Both methods showed similar anomalies for the AMJ, JAS, and OND quarters, demonstrating their robustness in capturing climate change signals (e.g., fig.E.20 for the SSP5-8.5 scenario and the horizon 2071-2100). However, during the JFM quarter, CNRM-ALADIN's convection led to more intense precipitation in the dynamical downscaling, resulting in divergent anomalies (e.g., Fig. E.20, first row). This reversed the climate change trend in the JFM period, slightly mitigating the drying signal projected by CNRM-ESM2-1.

Appendix F. Future dry season precipitation trends over La Réunion according to dynamical downscaling

Dry season precipitation trends from CNRM-ALADIN (Fig. F.21) show similar patterns to the median of the 22 statistically downscaled CMIP6 models over La Réunion (Fig. 14). Differences include greater contrast between grid points with CNRM-ALADIN (which makes sense compared to a median of models), drier trends over the extreme northwestern coast with CNRM-ALADIN, and stronger model internal variability under the SSP1-2.6 scenario with CNRM-ALADIN, while multi-model ensemble trends are more stable across the 21^st century.

(a) CNRM-ALADIN JFM (b) CNRM-BC-WT JFM (c) CNRM JFM

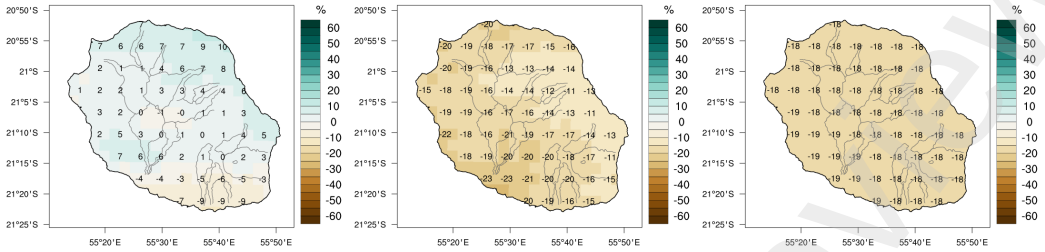

(d) CNRM-ALADIN AMJ (e) CNRM-BC-WT AMJ (f) CNRM AMJ

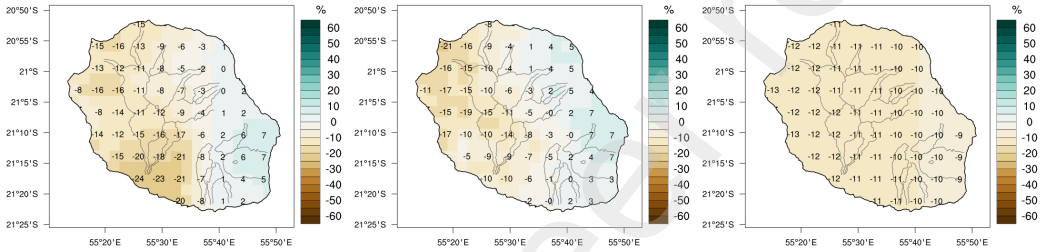

(g) CNRM-ALADIN JAS (h) CNRM-BC-WT JAS (i) CNRM JAS

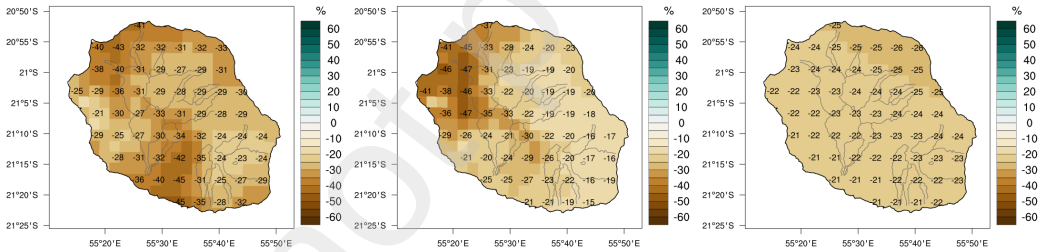

(j) CNRM-ALADIN OND (k) CNRM-BC-WT OND (l) CNRM OND

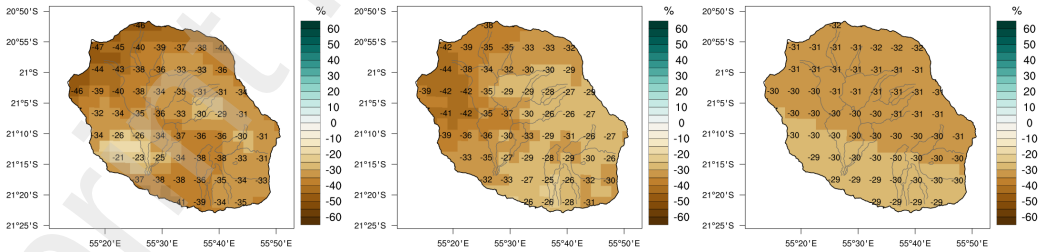

Figure E.20: Comparison of downscaling methods for La Réunion Island at 0.03° resolution, focusing on the case of CNRM-ESM2-1. The figure depicts precipitation anomalies (%) in the SSP5-8.5 scenario for the 2071-2100 period relative to 1981-2010. The color palette indicates the magnitude of anomalies. Rows 1 to 4 represent the four trimesters (JFM, AMJ, JAS, OND). Column 1 shows Dynamical Downscaling with CNRM-ALADIN and CDF-t Bias Correction at 0.03° resolution. Column 2 displays Statistical Downscaling of CNRM-ESM2-1 using weather types (BC-WT) at 0.03° resolution. Column 3 presents CNRM-ESM2-1 interpolated at 0.03° resolution.

(a) SSP1-2.6 2041-2070

(b) SSP1-2.6 2071-2100

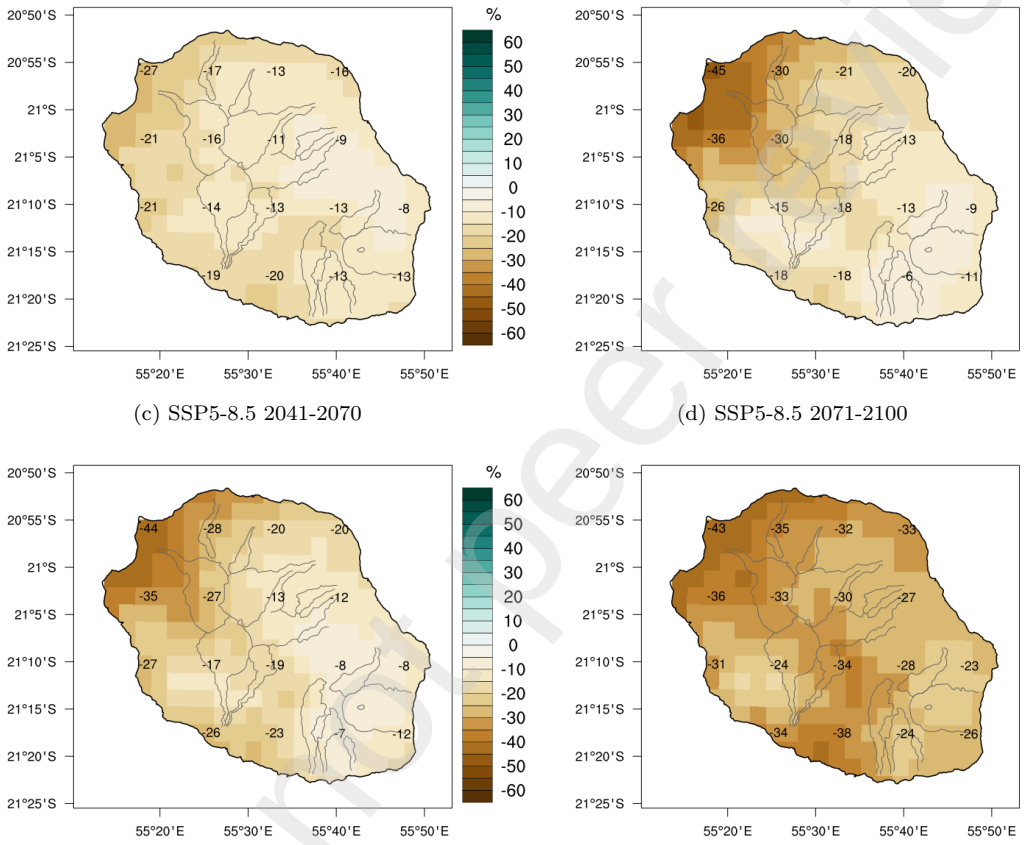

(c) SSP5-8.5 2041-2070

(d) SSP5-8.5 2071-2100

Figure F.21: Precipitation anomalies (%) resulting from dynamical downscaling using CNRM-ALADIN with CDF-t bias correction at 0.03° resolution. The figure illustrates precipitation anomalies for the dry season (June to November) under the SSP1-2.6 (row 1) and SSP5-8.5 (row 2) scenarios for the periods 2041-2070 (left column) and 2071-2100 (right column) compared to the reference 1981-2010 period. The color palette indicates the magnitude of anomalies.

Acknowledgements

We wish to express our gratitude to the following individuals for their invaluable contributions: Marie Lacoste of the CBN-CPIE Mascarin for her insightful input in defining the ombroclimate attribute; Fabrice Chauvin for his guidance with the cyclone tracking algorithm; Meteo-France's RCM team, including Pierre Nabat, Lola Corre, and Jean-François Guérémey, for their assistance with the regional model configurations; Guillaume Jumaux for supplying historical trend datasets over La Réunion and Mayotte; Jean-François Boyer for his work in creating comprehensive maps that summarize results across various IOC countries; and Kevin Lamy for his thorough internal review of our paper. Their collective expertise greatly enriched our research.

Data availability

The data presented in this study are available upon request from the corresponding author. The regional CNRM-ALADIN dataset will be made publicly available in due course at `climat.coi-ioc.org`.

CRediT authorship contribution statement

Marie-Dominique Leroux: Project administration, Conceptualization, Investigation, Formal analysis, Methodology, Data curation, Software, Resources, Supervision, Validation, Visualization, Writing - Original Draft, Writing - Review & Editing. **François Bonnardot**: Funding acquisition, Conceptualization, Investigation, Formal analysis, Methodology, Software, Data curation, Resources, Supervision, Visualization, Validation. **Samuel**

Somot: Methodology, Software, Resources, Writing - Original Draft. **Antoinette Alias**: Investigation, Software, Resources. **Stephason Kotomangazafy**: Investigation, Formal analysis, Software, Data curation. **Abdoul-Oikil Saïd Ridhoine**: Investigation, Formal analysis, Software, Data curation. **Philippe Veerabadren**: Investigation, Formal analysis, Software, Data curation. **Vincent Amélie**: Investigation, Formal analysis, Software, Data curation.

Declaration of Competing Interest

The authors declare that they have no known competing financial interests or personal relationships that could have appeared to influence the work reported in this paper.

Declaration of Generative AI and AI-assisted technologies in the writing process

During the preparation of this manuscript the main author used ChatGPT in order to improve the readability of some sentences and reduce the number of words. After using this tool, the main author reviewed and edited the content as needed and takes full responsibility for the content of the publication.

Funding

This research was supported by AdaptAction, a program developed by the AFD Group.

Abbreviations

The following abbreviations are used in this manuscript:

ACE	Accumulated Cyclone Energy
AR	Assessment Report
BRIO	Building Resilience in the Indian Ocean
BT	Best Track
CBN-CPIE Mascarin	National Botanical Conservatory Mascarin
CDF	Cumulative Distribution Function
CMIP	Coupled Model Inter-comparison Project
CORDEX	Coordinated Regional Climate Downscaling Experiment
ECS	Equilibrium climate sensitivity
ETP	Evapotranspiration
EUR	Easily Usable Reserve
GCM	Global Climate Model
GWL	Global Warming Level
IOC	Indian Ocean Commission
IPCC	Intergovernmental Panel on Climate Change
ITC	Intense Tropical Cyclone
ITCZ	InterTropical Convergence Zone
PDI	Power Dissipation Index
QQ	Quantile-quantile
RCM	Regional Climate Model
RCP	Representative Concentration Pathway
RH	Relative Humidity

RR	Precipitation
RSMC	Regional Specialized Meteorological Center
SSP	Shared Socioeconomic Pathway
SIDS	Small Island Developing States
SST	Sea Surface Temperature
SWIO	Southwest Indian Ocean
TC	Tropical Cyclone
TCR	Transient Climate Response
TS	Tropical Storm
TN	Minimum Temperature
TX	Maximum Temperature
UR	Usable Reserve
VITC	Very Intense Tropical Cyclone

References

[1] Allan, R., Pereira, L., Smith, M., 1998. Crop evapotranspiration-Guidelines for computing crop water requirements-FAO Irrigation and drainage paper 56. volume 56.

[2] Andriaandy, J.R., Randriamifidy, F.M., Andrianavony, J.K., 2023. Heat and Economics: Climate Change's Influence on Madagascar's GDP Online at `https://mpra.ub.uni-muenchen.de/118582/`.

[3] Ayat, H., Evans, J.P., Behrangi, A., 2021. How do different sensors impact imerg precipitation estimates during hurricane days? Remote Sensing of Environment 259, 112417. URL: `https://www.`

sciencedirect.com/science/article/pii/S0034425721001358, doi:https://doi.org/10.1016/j.rse.2021.112417.

[4] Bell, G.D., Chelliah, M., 2006. Leading tropical modes associated with interannual and multidecadal fluctuations in North Atlantic hurricane activity. J. Climate 19, 590–612.

[5] Bell, G.D., Coauthors, 2000. Climate assessment for 1999. Bull. Amer. Meteor. Soc. 81, S1–S50.

[6] Bessafi, M., Morel, B., Luk, J.D.L.S., Chabriat, J.P., Jeanty, P., 2013. A Method for Mapping Monthly Solar Irradiation Over Complex Areas of Topography: Réunion Island's Case Study., in: Springer, Climate Smart Technologies - Integrating Renewable Energy and Energy Efficiency in Mitigation and Adaptation Responses. In: Leal Filho W., Mannke F., Mohee R., Schulte V., Surroop D. (eds). volume Climate Change Management, pp. 295–306. URL: http://link.springer.com/chapter/10.1007/978-3-642-37753-2_22.

[7] Bloemendaal, N., de Moel, H., Martinez, A.B., Muis, S., Haigh, I.D., van der Wiel, K., Haarsma, R.J., Ward, P.J., Roberts, M.J., Dullaart, J.C.M., Aerts, J.C.J.H., 2022. A globally consistent local-scale assessment of future tropical cyclone risk. Science Advances 8, eabm8438. doi:10.1126/sciadv.abm8438.

[8] Boé, J., Somot, S., Corre, L., Nabat, P., 2020. Large discrepancies in summer climate change over europe as projected by global and regional

climate models: causes and consequences. Climate Dynamics 54, 2981–3002.

[9] Bérard, A., 2021. Changements futurs de la ressource en eau des sols à La Réunion sousculture de canne à sucre. Master thesis. Ecole Nationale de la Météorologie, IENM.

[10] Caillaud, C., Somot, S., Alias, A., Bernard-Bouissières, I., Fumière, Q., Laurantin, O., Seity, Y., Ducrocq, V., 2021. Modelling Mediterranean heavy precipitation events at climate scale: an object-oriented evaluation of the CNRM-AROME convection-permitting regional climate model. Clim. Dyn. 56, 1717–1752. URL: https://doi.org/10.1007/s00382-020-05558-y.

[11] Camargo, S.J., Sobel, A.H., 2005. Western North Pacific tropical cyclone intensity and ENSO. J. Climate 18, 2996–3006.

[12] Camargo, S.J., Wing, A.A., 2016. Tropical cyclones in climate models. Wiley Interdisciplinary Reviews: Climate Change 7, 211–237.

[13] Cannon, A.J., Alford, H., Shrestha, R.R., Kirchmeier-Young, M.C., Najafi, M.R., 2022. Canadian large ensembles adjusted dataset version 1 (canleadv1): Multivariate bias-corrected climate model outputs for terrestrial modelling and attribution studies in north america. Geoscience Data Journal 9, 288–303. URL: https://rmets.onlinelibrary.wiley.com/doi/abs/10.1002/gdj3.142, doi:https://doi.org/10.1002/gdj3.142.

[14] Cattiaux, J., Chauvin, F., Bousquet, O., Malardel, S., Tsai, C.L., 2020. Projected changes in the Southern Indian Ocean cyclone activity assessed from high-resolution experiments and CMIP5 models. J. Climate 33 (12), 4975–4991. doi:10.1175/jcli-d-19-0591.1.

[15] Chand, S., Walsh, K.J.E., C.S., Kossin, J.P., Tory, K.J., Wehner, M.F., Chan, J.C.L., Klotzbach, P.J., Dowdy, A.J., Bell, S.S., Ramsay, H.A., Murakami, H., 2022. Declining tropical cyclone frequency under global warming. Nat. Clim. Chang. 12, 655–661. doi:https://doi.org/10.1038/s41558-022-01388-4.

[16] Chauvin, F., Douville, H., Ribes, A., 2017. Atlantic tropical cyclones water budget in observations and CNRM-CM5 model. Clim. Dyn. 49(11–12), 4009–4021. doi:10.1007/s00382-017-3559-3.

[17] Chauvin, F., Pilon, R., Palany, P., Madani, A.B., 2020. Future changes in Atlantic hurricanes with the rotated-stretched ARPEGE-Climat at very high resolution. Clim. Dyn. 54, 947–972. doi:10.1007/s00382-019-05040-4.

[18] Chauvin, F., Royer, J.F., Déqué, M., 2006. Response of hurricane-type vortices to global warming as simulated by ARPEGE-Climat at high resolution. Clim. Dyn. 27, 377–399. doi:10.1007/s00382-006-0135-7.

[19] Daloz, A.S., Chauvin, F., Roux, F., 2012. Impact of the configuration of stretching and ocean–atmosphere coupling on tropical cyclone activity in the variable-resolution GCM ARPEGE. Clim. Dyn. 39, 2343–2359. doi:10.1007/s00382-012-1561-3.

[20] Done, J.M., Holland, G.J., Bruyère, C.L., Leung, L.R., Suzuki-Parker, A., 2015. Modeling high-impact weather and climate: lessons from a tropical cyclone perspective. Climatic Change 129, 381–395.

[21] Douglass, K., Cooper, J., 2020. Archaeology, environmental justice, and climate change on islands of the caribbean and southwestern indian ocean. Proceedings of the National Academy of Sciences 117, 8254–8262. doi:10.1073/pnas.1914211117.

[22] Doury, A., Somot, S., Gadat, S., Ribes, A., Corre, L., 2023. Regional climate model emulator based on deep learning: concept and first evaluation of a novel hybrid downscaling approach. Clim. Dyn. 60, 1751–1779. URL: https://doi.org/10.1007/s00382-022-06343-9, doi:10.1007/s00382-022-06343-9.

[23] Douville, H., 1992. Utilisation d'un modèle numérique de terrain pour le calcul de champs pluviométriques en zone montagneuse. Application de la méthode à l'île de La Réunion. Technical Report. Météo-France/Direction Interrégionale pour l'Océan Indien.

[24] Dvorak, V., 1984. Tropical cyclone intensity analysis using satellite data. NOAA Tech. Rep. NESDIS 11.

[25] Emanuel, K.A., 1987. The dependence of hurricane intensity on climate. Nature 326, 483–485.

[26] Eyring, V., Bony, S., Meehl, G.A., Senior, C.A., Stevens, B., Stouffer, R.J., Taylor, K.E., 2016. Overview of the coupled

model intercomparison project phase 6 (cmip6) experimental design and organization. Geoscientific Model Development 9, 1937–1958. URL: https://gmd.copernicus.org/articles/9/1937/2016/, doi:10.5194/gmd-9-1937-2016.

[27] Fitchett, J.M., 2018. Recent emergence of cat5 tropical cyclones in the south indian ocean. South African Journal of Science 114. URL: https://sajs.co.za/article/view/4426, doi:10.17159/sajs.2018/4426.

[28] Forster, P., Storelvmo, T., Armour, K., Collins, W., Dufresne, J.L., Frame, D., Lunt, D., Mauritsen, T., Palmer, M., Watanabe, M., Wild, M., Zhang, H., 2021. The Earth's Energy Budget, Climate Feedbacks, and Climate Sensitivity. Cambridge University Press, Cambridge, United Kingdom and New York, NY, USA. p. 923–1054. doi:10.1017/9781009157896.009.

[29] Fox-Kemper, B., Hewitt, H., Xiao, C., Aoalgeirsdóttir, G., Drijfhout, S., Edwards, T., Golledge, N., Hemer, M., Kopp, R., Krinner, G., Mix, A., Notz, O., Nowicki, S., Nurhati, I., Ruiz, L., Sallée, J.B., Slangen, A., Yu, Y., 2021. Cryosphere and Sea Level Change. Cambridge University Press, Cambridge, United Kingdom and New York, NY, USA. p. 1211–1362. URL: https://www.ipcc.ch/report/ar6/wg1/downloads/report/IPCC_AR6_WGI_Chapter09.pdf, doi:10.1017/9781009157896.011.

[30] Funk, C., Peterson, P., Landsfeld, M., Pedreros, D., Verdin, J., Shukla, S., Husak, G., Rowland, J., Harrison, L., Hoell, A., Michaelsen, J.,

2015. The climate hazards infrared precipitation with stations — a new environmental record for monitoring extremes. Scientific Data 2, 150066.

[31] Goldenson, N., Leung, L.R., Mearns, L.O., Pierce, D.W., Reed, K.A., Simpson, I.R., Ullrich, P., Krantz, W., Hall, A., Jones, A., Rahimi, S., 2023. Use-inspired, process-oriented gcm selection: Prioritizing models for regional dynamical downscaling. Bulletin of the American Meteorological Society doi:https://doi.org/10.1175/BAMS-D-23-0100.1.

[32] Guhathakurta, P., Wagh, N., 2022. Analysis of droughts in south-west indian ocean countries using spi and spei and their relationship with global sst. JNRD - Journal of Natural Resources and Development 12, 60–81. URL: https://journals.ub.uni-koeln.de/index.php/JNRD/article/view/899, doi:10.18716/ojs/jnrd/2022.12.04.

[33] Hausfather, Z., Marvel, K., Schmidt, G.A., Nielsen-Gammon, J.W., Zelinka, M., 2022. Climate simulations: Recognize the 'hot model'problem. Nature 605, 26–29.

[34] Hersbach, H., Bell, W., Berrisford, P., Horányi, A., J., M.S., Nicolas, J., Radu, R., Schepers, D., Simmons, A., Soci, C., Dee, D., 2019. Global reanalysis: goodbye ERA-Interim, hello ERA5. Meteorology 159, 17–24. URL: https://www.ecmwf.int/node/19027, doi:10.21957/vf291hehd7.

[35] Huffman, G., Bolvin, D., Nelkin, E., Tan, J., 2019. Integrated Multi-satellitE Retrievals for GPM (IMERG). Technical Documentation. NASA Goddard Space Flight Center.

[36] IPCC, 2021. Climate Change 2021: The Physical Science Basis. Contribution of Working Group I to the Sixth Assessment Report of the Intergovernmental Panel on Climate Change. volume In Press. Cambridge University Press, Cambridge, United Kingdom and New York, NY, USA. doi:10.1017/9781009157896.

[37] IPCC, 2022. Climate Change 2022: Impacts, Adaptation, and Vulnerability. Contribution of Working Group II to the Sixth Assessment Report of the Intergovernmental Panel on Climate Change. Cambridge University Press, Cambridge, United Kingdom and New York, NY, USA. doi:10.1017/9781009325844.

[38] Jumaux, G., Quetelard, H., Roy, D., 2011. Atlas Climatique de La Réunion. Technical Report. Météo-France/Direction Interrégionale pour l'Océan Indien.

[39] Knapp, K.R., Kruk, M.C., Levinson, D.H., Diamond, H.J., Neumann, C.J., 2010. The international best track archive for climate stewardship (ibtracs): Unifying tropical cyclone data. Bull. Amer. Meteor. Soc. 91, 363 – 376. doi:https://doi.org/10.1175/2009BAMS2755.1.

[40] Knutson, T., Camargo, S.J., Chan, J.C., Emanuel, K., Ho, C.H., Kossin, J., Mohapatra, M., Satoh, M., Sugi, M., Walsh, K., 2020. Tropical cyclones and climate change assessment: Part II: Projected response to anthropogenic warming. Bull. Amer. Meteor. Soc. 101, E303–E322.

[41] Kossin, J., Knapp, K., Olander, T., Velden, C., 2020. Global increase in

major tropical cyclone exceedance probability over the past four decades. Proceedings of the National Academy of Sciences 117(22), 11975–11980.

[42] Kossin, J.P., Emanuel, K.A., Vecchi, G.A., 2014. The poleward migration of the location of tropical cyclone maximum intensity. Nature 509, 349–352.

[43] Krishna Prabhakar, S.V.R., 2022. Implications of Regional Droughts and Transboundary Drought Risks on Drought Monitoring and Early Warning: A Review. Climate 10. URL: https://www.mdpi.com/2225-1154/10/9/124.

[44] Lamy, K., Tran, A., Portafaix, T., Leroux, M., Baldet, T., 2023. Impact of regional climate change on the mosquito vector Aedes albopictus in a tropical island environment: La Réunion. Science of The Total Environment 875, 162484. doi:https://doi.org/10.1016/j.scitotenv.2023.162484.

[45] Lavaysse, C., Vrac, M., Drobinski, P., Lengaigne, M., Vischel, T., 2012. Statistical downscaling of the French Mediterranean climate: Assessment for present and projection in an anthropogenic scenario. Nat. Hazards Earth Syst. Sci. 12, 651–670. doi:doi:10.5194/nhess-12-651-2012.

[46] Leroux, M.D., Meister, J., Mekies, D., Dorla, A.L., Caroff, P., 2018. A climatology of southwest indian ocean tropical systems: Their number, tracks, impacts, sizes, empirical maximum potential intensity, and intensity changes. Journal of Applied Meteorol-

ogy and Climatology 57, 1021–1041. URL: https://doi.org/10.1175/JAMC-D-17-0094.1, doi:10.1175/JAMC-D-17-0094.1, arXiv:https://doi.org/10.1175/JAMC-D-17-0094.1.

[47] Lu, B., Ren, H.L., 2020. What caused the extreme indian ocean dipole event in 2019? Geophys. Res. Lett. 47, e2020GL087768. doi:https://doi.org/10.1029/2020GL087768.

[48] Lucas-Picher, P., Argüeso, D., Brisson, E., Tramblay, Y., Berg, P., Lemonsu, A., Kotlarski, S., Caillaud, C., 2021. Convection-permitting modeling with regional climate models: Latest developments and next steps. WIREs Climate Change 12, e731. doi:https://doi.org/10.1002/wcc.731.

[49] Meehl, G.A., Senior, C.A., Eyring, V., Flato, G., Lamarque, J.F., Stouffer, R.J., Taylor, K.E., Schlund, M., 2020. Context for interpreting equilibrium climate sensitivity and transient climate response from the cmip6 earth system models. Science Advances 6, eaba1981. doi:10.1126/sciadv.aba1981.

[50] Meinshausen, M., Nicholls, Z.R.J., Lewis, J., Gidden, M.J., Vogel, E., Freund, M., Beyerle, U., Gessner, C., Nauels, A., Bauer, N., Canadell, J.G., Daniel, J.S., John, A., Krummel, P.B., Luderer, G., Meinshausen, N., Montzka, S.A., Rayner, P.J., Reimann, S., Smith, S.J., van den Berg, M., Velders, G.J.M., Vollmer, M.K., Wang, R.H.J., 2020. The shared socio-economic pathway (ssp) greenhouse gas concentrations and their extensions to 2500. Geoscientific Model Development 13,

3571–3605. URL: https://gmd.copernicus.org/articles/13/3571/2020/, doi:10.5194/gmd-13-3571-2020.

[51] Michelangeli, P., Vrac, M., Loukos, H., 2009. Probabilistic downscaling approaches: Application to wind cumulative distribution functions. Geophys. Res. Lett. 36, L11708. doi:doi:10.1029/2009GL038401.

[52] Murakami, H., Sugi, M., 2010. Effect of model resolution on tropical cyclone climate projections. Sola 6, 73–76. URL: https://api.semanticscholar.org/CorpusID:724477.

[53] Murakami, H., Wang, Y., Yoshimura, H., Mizuta, R., Sugi, M., Shindo, E., Adachi, Y., Yukimoto, S., Hosaka, M., Kusunoki, S., Ose, T., Kitoh, A., 2012. Future Changes in Tropical Cyclone Activity Projected by the New High-Resolution MRI-AGCM. J. Climate 25, 3237–3260. URL: https://journals.ametsoc.org/view/journals/clim/25/9/jcli-d-11-00415.1.xml, doi:https://doi.org/10.1175/JCLI-D-11-00415.1.

[54] Nabat, P., Somot, S., Cassou, C., Mallet, M., Michou, M., Bouniol, D., Decharme, B., Drugé, T., Roehrig, R., Saint-Martin, D., 2020. Modulation of radiative aerosols effects by atmospheric circulation over the Euro-Mediterranean region. Atmos. Chem. Phys. 20, 8315–8349. URL: https://acp.copernicus.org/articles/20/8315/2020/, doi:10.5194/acp-20-8315-2020.

[55] Nematchoua, M.K., Ricciardi, P., Orosa, J.A., Buratti, C., 2018. A detailed study of climate change and some vulnerabilities in indian ocean:

A case of madagascar island. Sustainable Cities and Society 41, 886–898. doi:https://doi.org/10.1016/j.scs.2018.05.040.

[56] Omranian, E., Sharif, H.O., Tavakoly, A.A., 2018. How well can global precipitation measurement (gpm) capture hurricanes? case study: Hurricane harvey. Remote Sensing 10. URL: https://www.mdpi.com/2072-4292/10/7/1150, doi:10.3390/rs10071150.

[57] O'Neill, B.C., Tebaldi, C., van Vuuren, D.P., Eyring, V., Friedlingstein, P., Hurtt, G., Knutti, R., Kriegler, E., Lamarque, J.F., Lowe, J., Meehl, G.A., Moss, R., Riahi, K., Sanderson, B.M., 2016. The Scenario Model Intercomparison Project (ScenarioMIP) for CMIP6. Geoscientific Model Development 9, 3461–3482. URL: https://gmd.copernicus.org/articles/9/3461/2016/, doi:10.5194/gmd-9-3461-2016.

[58] Palmer, T.E., McSweeney, C.F., Booth, B.B.B., Priestley, M.D.K., Davini, P., Brunner, L., Borchert, L., Menary, M.B., 2023. Performance-based sub-selection of cmip6 models for impact assessments in europe. Earth System Dynamics 14, 457–483. URL: https://esd.copernicus.org/articles/14/457/2023/, doi:10.5194/esd-14-457-2023.

[59] Rija, F., 2019. Renforcement du Service d'Information Climatique MAPROOM de Madagascar pour répondre aux besoins des secteurs clés de développement. Technical Report. Antananarivo: Meteo Madagascar.

[60] Roberts, M.J., Vidale, P.L., Mizielinski, M.S., Demory, M.E., Schiemann, R., Strachan, J., Hodges, K., Bell, R., Camp, J., 2015. Tropical

cyclones in the upscale ensemble of high-resolution global climate models. Journal of Climate 28, 574 – 596. doi:https://doi.org/10.1175/JCLI-D-14-00131.1.

[61] Rummukainen, M., 2016. Added value in regional climate modeling. WIREs Climate Change 7, 145–159. doi:https://doi.org/10.1002/wcc.378.

[62] Scafetta, N., 2021. Testing the cmip6 gcm simulations versus surface temperature records from 1980–1990 to 2011–2021: High ecs is not supported. Climate 9. URL: https://www.mdpi.com/2225-1154/9/11/161, doi:10.3390/cli9110161.

[63] Scafetta, N., 2023. Cmip6 gcm validation based on ecs and tcr ranking for 21st century temperature projections and risk assessment. Atmosphere 14. URL: https://www.mdpi.com/2073-4433/14/2/345, doi:10.3390/atmos14020345.

[64] Séférian, R., Nabat, P., Michou, M., Saint-Martin, D., Voldoire, A., et al., J.C., 2019. Evaluation of CNRM Earth System model, CNRM-ESM2-1: role of Earth system processes in present-day and future climate. Journal of Advances in Modeling Earth Systems 11, 4182–4227. doi:10.1029/2019MS001791.

[65] Tang, C., Morel, B., Singh, S., Graillet, A., Pergaud, J., Mugenga, R.I., Baraka, L., Leroux, M.D., Jeanty, P., Delsaut, M., Cunden, T.S., Beeharry, G.K., Lollchund, R., 2023. High-resolution dynamical downscaling experiment outputs data over re-

union and mauritius islands in the south-west indian ocean. Data in Brief , 109665URL: https://www.sciencedirect.com/science/article/pii/S2352340923007503, doi:https://doi.org/10.1016/j.dib.2023.109665.

[66] Taranu, I.S., Somot, S., Alias, A., Boé, J., Delire, C., 2023. Mechanisms behind large-scale inconsistencies between regional and global climate model-based projections over europe. Climate Dynamics 60, 3813–3838.

[67] Thompson, C., Barthe, C., Bielli, S., Tulet, P., Pianezze, J., 2021. Projected characteristic changes of a typical tropical cyclone under climate change in the south west indian ocean. Atmosphere 12. URL: https://www.mdpi.com/2073-4433/12/2/232, doi:10.3390/atmos12020232.

[68] Velden, C., Harper, B., Wells, F., II, J.L.B., Zehr, R., Olander, T., Mayfield, M., Guard, C., Lander, M., Edson, R., Avila, L., Burton, A., Turk, M., Kikuchi, A., Christian, A., Caroff, P., McCrone, P., 2006. The Dvorak Tropical Cyclone Intensity Estimation Technique: A Satellite-Based Method that Has Endured for over 30 Years. Bull. Amer. Meteor. Soc. 87, 1195–1210.

[69] Vrac, M., Drobinski, P., Merlo, A., Herrmann, M., Lavaysse, C., Li, L., Somot, S., 2012. Dynamical and statistical downscaling of the French Mediterranean climate: Uncertainty assessment. Nat. Hazards Earth Syst. Sci. 12, 2769–2784. doi:doi:10.5194/nhess-12-2769-2012.

[70] Walsh, K.J., McBride, J.L., Klotzbach, P.J., Balachandran, S., Camargo, S.J., Holland, G., Knutson, T.R., Kossin, J.P., Lee, T.c., So-

bel, A., Sugi, M., 2016. Tropical cyclones and climate change. WIREs Climate Change 7, 65–89. doi:https://doi.org/10.1002/wcc.371.

[71] Weiskopf, S.R., Cushing, J.A., Morelli, T., Myers, B.J.E., 2021. Climate change risks and adaptation options for Madagascar. Ecology and Society 26(4), 36. URL: https://doi.org/10.5751/ES-12816-260436.

[72] WMO, 2017. Global Guide to Tropical Cyclone Forecasting, World Meteorological Organization, WMO/TD-No. 1194, Geneva. URL: https://cyclone.wmo.int/pdf/Global-Guide-to-Tropical-Cyclone-Forecasting.pdf.

[73] Yu, C., Hu, D., Di, Y., Wang, Y., 2021. Performance evaluation of imerg precipitation products during typhoon lekima (2019). Journal of Hydrology 597, 126307. URL: https://www.sciencedirect.com/science/article/pii/S0022169421003541, doi:https://doi.org/10.1016/j.jhydrol.2021.126307.